REPORT DOCUMENTATION PAGE

Form Approved OMB No. 0704-0188

1. AGENCY USE ONLY (Leave blank)	2. REPORT DATE	3. REPORT TYPE AND DATES COVERED
	August 1995	Final Report

4. TITLE AND SUBTITLE

Investigation of Photorefractive Crystals

5. FUNDING NUMBERS

F6170894W0775

6. AUTHOR(S)

Dr. Serguey Odoulov

7. PERFORMING ORGANIZATION NAME(S) AND ADDRESS(ES)

Dynamic Holography Group, Institute of Physics
National Academy of Sciences
Science Ave 46,
Kiev 252 650
Ukraine

8. PERFORMING ORGANIZATION REPORT NUMBER

N/A

9. SPONSORING/MONITORING AGENCY NAME(S) AND ADDRESS(ES)

EOARD
PSC 802 BOX 14
FPO 09499-0200

10. SPONSORING/MONITORING AGENCY REPORT NUMBER

SPC 94-4099

11. SUPPLEMENTARY NOTES

12a. DISTRIBUTION/AVAILABILITY STATEMENT

Approved for public release; distribution is unlimited.

12b. DISTRIBUTION CODE

A

13. ABSTRACT (Maximum 200 words)

This report results from a contract tasking Dynamic Holography Group, Institute of Physics
National Academy of Sciences as follows: Investigate sillenite crystals and semiconductor photorefractive crystals, especially examining the effect of external AC and DC fields to improve the coupling strength and diffraction efficiency of the recorded gratings.

14. SUBJECT TERMS

EOARD

15. NUMBER OF PAGES

16. PRICE CODE
N/A

17. SECURITY CLASSIFICATION OF REPORT	18. SECURITY CLASSIFICATION OF THIS PAGE	19. SECURITY CLASSIFICATION OF ABSTRACT	20. LIMITATION OF ABSTRACT
UNCLASSIFIED	UNCLASSIFIED	UNCLASSIFIED	UL

E O A R D

Special contract SPC-94-4099

August 20, 1994 - August 20, 1995

Investigation of Photorefractive Crystals

FINAL REPORT

Principal investigator:

Serguey G. ODOULOV

Participating in research:

Konstantin V. SHCHERBIN

Alexander N. SHUMELYUK

Petro M. FOCHUK

Institute of Physics

National Academy of Sciences

Kiev, UKRAINE

CONTENT

INTRODUCTION

1. BEAM-COUPLING IN CADMIUM TELLURIDE CRYSTALS WITH NO APPLIED FIELD. CHARACTERIZATION OF CRYSTALS.

    1.1. Experimental set-up

    1.2. Intensity dependent photorefractive recording

    1.3. Spatial-frequency dependence of the gain factor

    1.4. Dynamics of grating recording and erasure in CdTe

    References

2. BEAM-COUPLING IN SEMICONDUCTOR PHOTOREFRACTIVE CRYSTALS WITH MOVING GRATINGS

    2.1. Two-beam-coupling spectra

    2.2. Discussion

        2.2.1. Thickness-dependent relaxation time

        2.2.2. Complicated spectra of several gratings

    2.3. Enchancement of beam-coupling by grating motion

    References

3. BEAM-COUPLING IN CdTe WITH EXTERNAL ELECTRIC FIELD

    3.1. Beam-coupling with high-frequency sinusoidal electric field.

    3.2. Beam-coupling with low-frequency sinusoidal and square-shaped electric field.

    3.3. "Net" gain due to beam-coupling in CdTe.

    References

CONCLUSIONS

INTRODUCTION

The purpose of this project was to investigate the photorefractive crystals with cubic symmetry. Both the sillenite type crystals and semiconductor materials [1.1], belonging to cubic classes of symmetry possess the best photorefractive sensitivity and assure the shortest response time as compared to other photorefractive materials. The disadvantage of these materials is in comparatively low light-induced refractive index change which is mainly due to their poor electrooptic quality. The particular aim of our project was to find the possible ways of improvement of the coupling strength and therefore of diffraction efficiency of the recorded dynamic grating.

This report describes how we tried to solve this problem and demonstrates the improvement which has been reached. In Conclusion we also point out some still existing questions and discuss possible further optimization of two-beam coupling in semiconductor photorefractive materials.

We selected as a material for our study Cadmium Telluride crystal [1.2] belonging to $\bar{4}3m$ point group class of symmetry. The background for this choice is the best electrooptic quality (largest $n^3 r_{eff}$ value within this group of noncentrosymmetric semiconductors) and preliminary information about possibility to grow high-resistant semiinsulating material. In same cases we study also Gallium Arsenide crystals to compare the results with this reference material. As distinct from photorefractive CdTe described in few previous publications we use the other type of dopant, namely germanium doped crystals. As it will be clear from the following description just this type

of doping and sufficiently high density of impurity centers allowed us to overcome the limitations due to rather long transport lengths and to get higher coupling strengths both with no applied field and with the AC applied field.

In this Report we first describe the experiments on characterization of CdTe:Ge as a photorefractive material, comparing the data measured by different techniques and evaluating such characteristics as dark and photoconductivity, lifetime-mobility product, trap density, diffusion length and Debye screening length. We describe further on the moving grating technique to study the dynamics of charge transport in these crystals. The same moving grating technique is used for the first time to improve the steady-state coupling strength in new photorefractive crystal ($Sn_2P_2S_6$) with two complimentary photorefractive gratings due to two species of charge carriers.

All these experiments are performed with no applied electric field to the crystal and we can define the optimum conditions for getting the largest beam-coupling and evaluate the best gain factor. And finally we turn to the experiments with the sinusoidal and square-wave AC fields and demonstrate a reasonably large gain factor (up to $\approx$ 6 cm^{-1}) for moderate electric field amplitude E $\approx$ 8.8 KV/cm.

1. BEAM-COUPLING IN CADMIUM TELLURIDE CRYSTALS WITH NO APPLIED FIELD. CHARACTERIZATION OF CRYSTALS.

The crystals studied were grown by Bridgman technique in Chernovtsy State University. They were deliberately germanium-doped and exhibited dark conductivity of order of 10^{-9} $(\text{Ohm}\times\text{cm})^{-1}$. The absorption spectrum (Fig. 1.1) clearly shows a characteristic shoulder due to the presence of impurity. In the same time the absorptivity at near infrared region of spectrum is obviously smaller then the reported data for other similar crystals [1.4,1.7] and is 1.2 cm^{-1} at 1.064 μm.

All samples have rectangular shape with typical dimensions $5\times5\times5$ mm^3 along $[1\bar{1}0]$, $[\bar{1}\,\bar{1}\,1]$, and $[11\bar{1}]$ - directions. The faces parallel to $(1\bar{1}0)$ and $(11\bar{1})$ planes were optically finished.

In all germanium-doped samples we have observed the pronounced photorefractive recording.

1.1. Experimental set-up.

To evaluate some solid-state parameters of the samples studied we measure the diffraction efficiency and gain factor in two-beam interaction arrangement. Figure 1.2 represents schematically the experimental set-up. The single-mode, single-frequency diode-pumped Nd^{3+}:YAG laser (1.064 μm) is used as a pump source. With lambda-half phase retarder and polarizer the output intensity of a laser could be varied within the interval 0.5W... 0.05 mW.

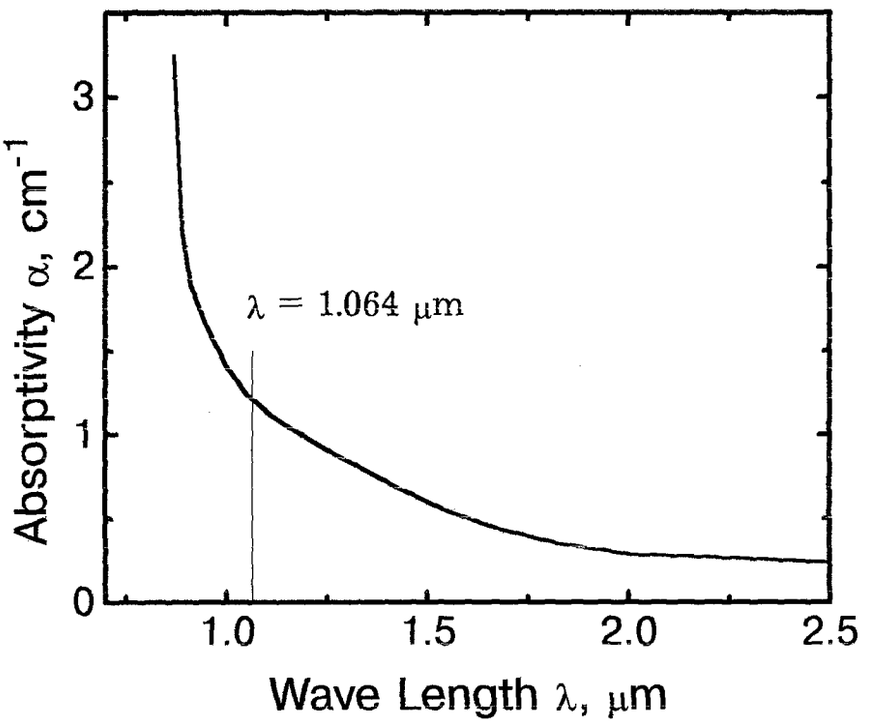

Fig. 1.1. Absorption spectrum of CdTe crystal.

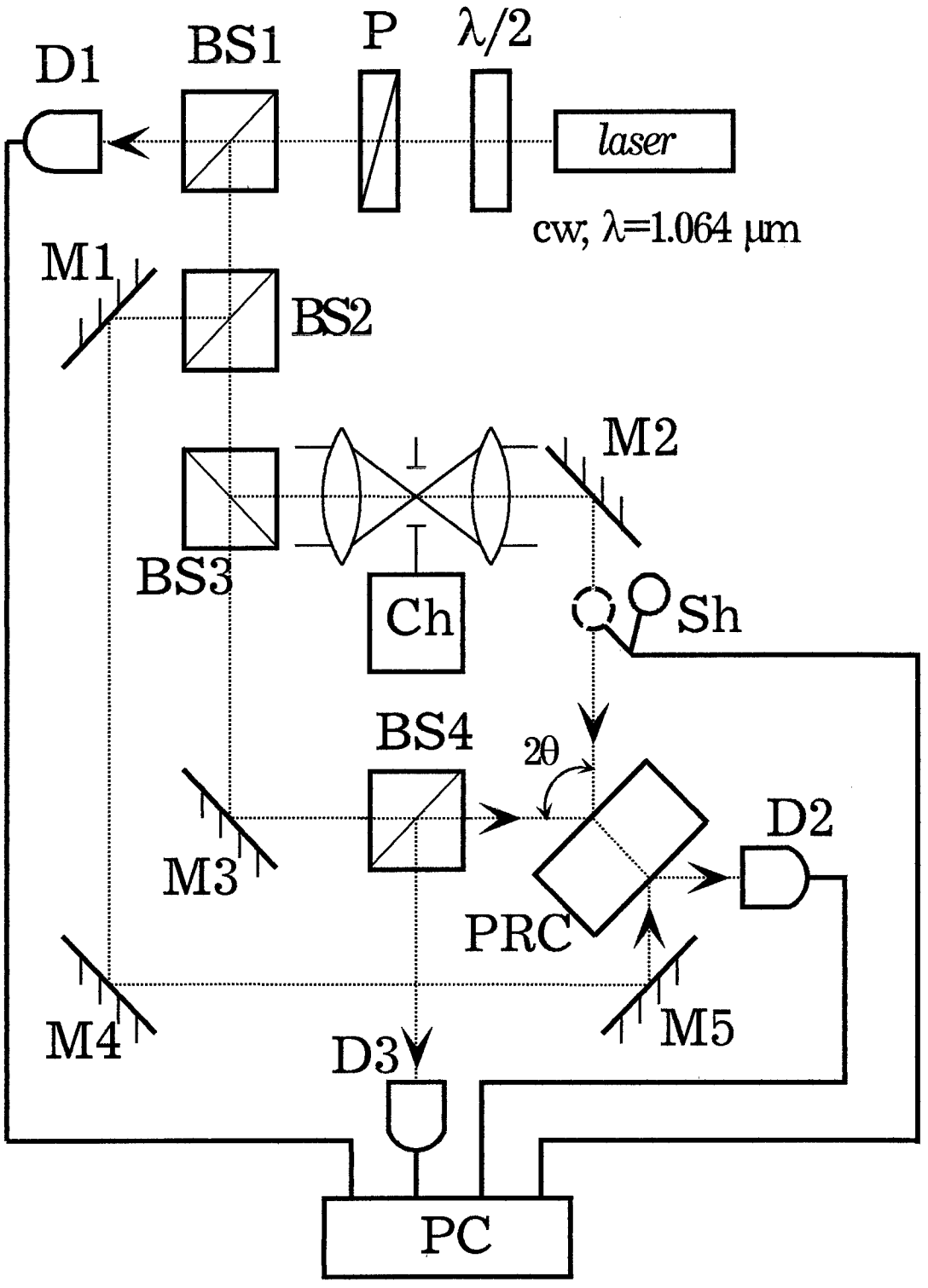

Fig. 1.2. Experimental set-up.

A fraction of incident beam deflected by the beam-splitter BS1 was continuously monitored by the detector D1.

Two beams recording a grating were formed by the beam-splitter BS3. After passing all optical elements two beams were coming to the input face of the sample with the intensity ratio 1:1 with accuracy not worse then 0.05. These beams impinge upon the sample at an angle 2θ thus recording a grating inside it.

To measure the diffraction efficiency and to read out this grating a third beam formed by a beamsplitter BS2 and mirrors M1, M4, and M5 was sent to the sample in direction opposite to that of one of two recording beams (precisely to beam reflected by a mirror M2). In such a way the Bragg matching condition for volume grating was automatically met. A part of the diffracted beam deflected by the beamsplitter BS4 was sent to the detector D3. The symmetric two-lens telescope was installed in one of two recording waves, with a chopper Ch placed exactly in focal plane of both lenses. This system allowed to stop one recording beam within less then 3 μs; it was used to study the writing-erasure cycles of the recorded dynamic grating.

To study the beam coupling we used the beam-splitter BS3 which assures the intensity ratio nearly 1:100. We measured the standard gain factor $\Gamma = (1/d)\times ln(I_S/I_{S0})$, where I_S and I_{S0} are the intensities of the output signal beam with and without the pump beam, respectively, and d is the interaction length inside the sample. The detector D2 placed behind the sample is measuring the intensity of the transmitted signal beam. The shutter Sh control

the presence of the pump beam. All the beams have gaussian intensity profile with the beam waist at the input face of the sample equal to 2.5 mm.

The control of all experimental parameters, data acquisition and treatment were performed by PC.

To study the interaction of copropagating waves two beams enter the sample through the same input face parallel to $(1\bar{1}0)$-plane, while to study the interaction of contrapropagating waves two beams enter the sample through opposite side faces parallel to $(11\bar{1})$ (see Fig. 1.3). In such a manner the grating vector $\vec{K}$ is kept parallel to $[11\bar{1}]$ direction and the polarization unit vectors of two recording waves are in plane of incidence. This geometry of interaction assures the largest possible effective electrooptic coefficient r_{eff} for transmission gratings recording, $r'_{333} \approx 1.1547\ r_{123}$ [1.5,1.11].

1.2. Intensity dependent photorefractive recording

The photorefractive grating appears as a result of spatial redistribution of the photoexcited carriers because of gradients of free-carrier density due to nonuniform illumination of the sample. The erasure of the grating is caused by the washing out of the space-charge because of finite conductivity of the material, dark conductivity as well as photoconductivity. In case of linear recombination of photoexcited carriers and pronounced photoconductivity both the excitation rate and the rate of charge relaxation are proportional to the light intensity; therefore the steady-state grating efficiency and gain factor are independent of light intensity. This is not true for the case of strong dark

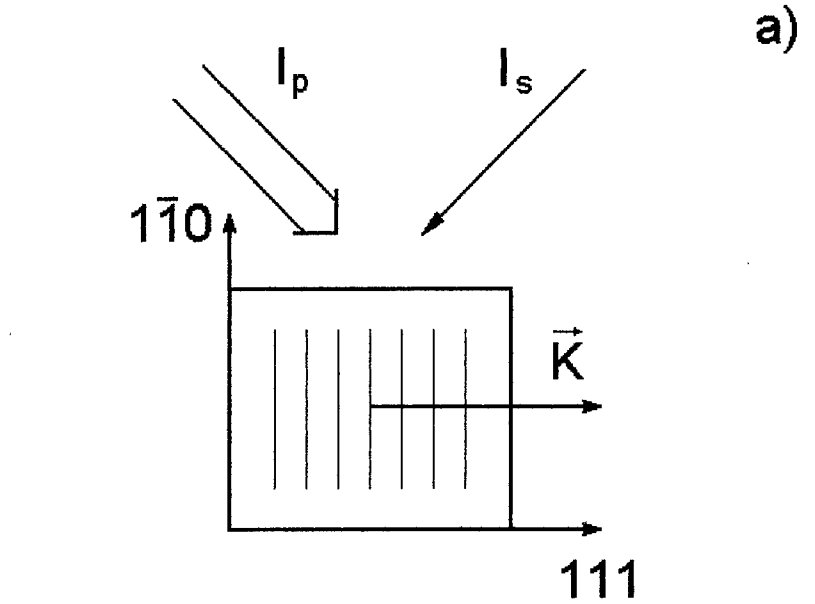

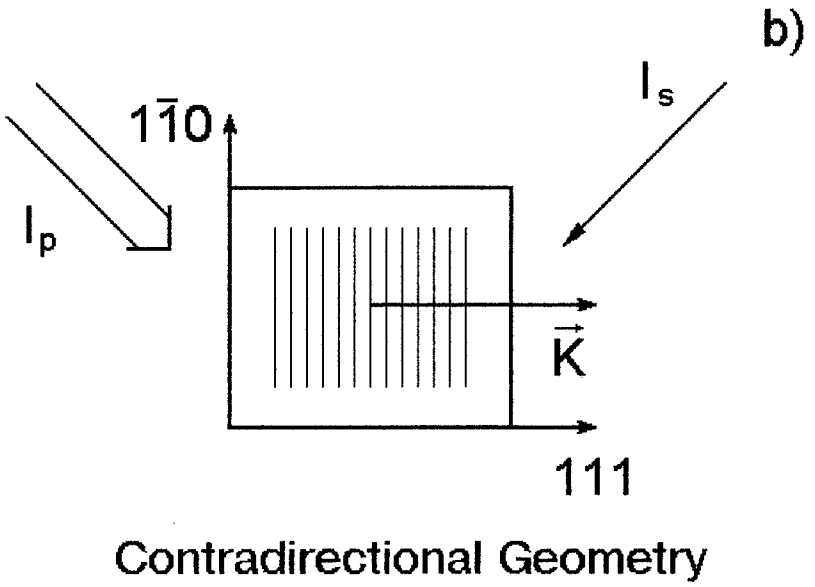

Fig. 1.3. Schematic of recording of the transmission (a) and reflaction (b) gratings.

conductivity, comparable to photoconductivity when the gain factor (and diffraction efficiency) are functions of light intensity

$$\Gamma = \Gamma_0 \times \frac{1}{1+\frac{\sigma_D}{\sigma_{Ph}}} = \Gamma_0 \times \frac{1}{1+\frac{\sigma_D}{\kappa I}}, \qquad (1.1)$$

with σ_D and $\sigma_{Ph} = \kappa I$ standing for the dark and photoconductivity of the material, κ is the specific photoconductivity.

Figure 1.4 represents such an intensity dependence of the gain factor Γ measured at grating spacing $\Lambda \approx 2.6$ μm. The intensities given here and in what follows are the averaged integral intensities with the Fresnel reflection at the input face taken into account. The gain factor is practically saturated for the intensities larger then 20 mW/cm^2. The solid line is the best theoretical fit (Eq. 1.1) with $\Gamma_0 = 0.4$ cm^{-1} and $\frac{\sigma_D}{\kappa} = 3$ mW/cm^2. With the directly measured value of dark conductivity $\sigma_D \approx 10^{-9}$ (Ohm×cm)$^{-1}$ one can evaluate the specific photoconductivity $\kappa \approx 3.3\times10^{-7}$ cm/V^2. The directly mesured photoconductivity at intensity I ≈ 90 mW/cm^2 give us the $\kappa \approx 10^{-7}$ cm/V^2 what is sufficiently close to this value.

Within approximation of linear recombination it is possible to present the photoconductivity in a following way

$$\sigma_{Ph} = \kappa I = (e\mu\tau\Phi\alpha I / h\nu), \qquad (1.2)$$

where e is the electron charge, μ is the charge mobility, τ is the carrier lifetime, Φ is the quantum efficiency, hν is the quantum energy.

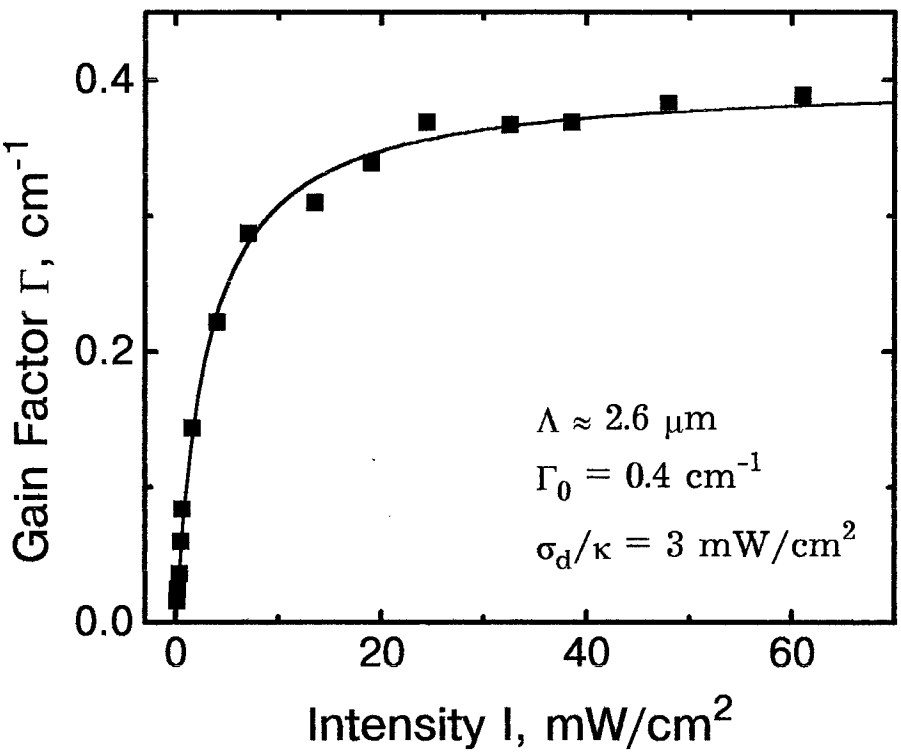

Fig. 1.4. Intensity dependence of the gain factor.

Using Eq. 1.2 it is possible to evaluate the product $\mu\tau$ from the experimental data.

$$\mu\tau = \left(\kappa h\nu / e\Phi\alpha\right). \qquad (1.3)$$

Putting $\Phi = 1$, $h\nu = 1.17$ eV and $\alpha \approx 1.2$ cm^{-1} at 1.064 μm we get $\mu\tau \approx 3.2\times10^{-7}$ cm^2/V. This value is in reasonable agreement with other estimates (see, e.g., [1.10,1.12]) and with handbook values for electrons $\tau = 5\times10^{-10}$ s and $\mu = 10^3$ cm^2/Vs or $\mu\tau = 5\times10^{-7}$ cm^2/V.

1.3. Spatial-frequency dependence of the gain factor

It is well known that the amplitude of the space-charge grating in diffusion process of recording is increasing with the diminishing grating spacing Λ until the Debye screening length l_S is reached. The grating spacing dependence of the gain factor predicted by theory [1.13] is

$$\Gamma = -\frac{4\pi^2 n_0^3 r_{eff}}{\lambda \cos\theta'} \times \frac{k_B T}{e} \times \frac{\Lambda}{\Lambda^2 + l_s^2} \times \xi(\Lambda), \qquad (1.4)$$

where n_0 is the refractive index, θ' is the pump halfangle inside the crystal, k_B is the Bolzmann constant, T is the absolute temperature, and ξ is electron-hole competition factor taking into account a possible compensation of the main grating by the grating formed with carriers of opposite sign. This factor in general is spatial-frequency dependent. The maximum in grating spacing dependence of the gain factor corresponds to Debye screening length l_S; this characteristic length in turn is a function of the efficient density of traps N_E, participating in volume space-charge formation

$$l_S = \sqrt{\frac{4\pi^2 \varepsilon \varepsilon_0 k_B T}{e^2 N_E}}, \qquad (1.5)$$

where ε and ε_0 are the dielectric constants of the medium and vacuum, respectively, $N_E = \frac{N_D^+ (N_D - N_D^+)}{N_D}$, and N_D and N_D^+ are the full density of donors and the density of ionized donors (traps).

To evaluate the Debye screening length and the density of trap centers in the investigated samples we measure the grating spacing dependence of the

gain factor Γ in two-beam coupling experiment (Fig. 1.5). With the increasing angle between two writing beams the value of the gain factor is also increasing, for transmission geometry (squares ■) as well as for reflection geometry (diamonds ◆). For nearly counterpropagating recording beams the spatial frequency of the recorded grating practically is not changing with the pump angle because of strong refraction of cadmium telluride (n = 2.82) [1.14], and thus Λ is close to 0.19 μm. These experimental values are presented in Fig. 1.5.

It should be noted in addition that the efficient electrooptic constants are different for the transmission and for reflection geometries. For interaction of counterpropagating waves (Fig. 3b) the effective constant $r'_{223} \approx 0.5674 \times r_{123}$ is involved whereas for copropagating waves the other constant, $r'_{333} \approx -1.1547 \times r_{123}$ is important. When changing the pump angle θ' inside the crystal of $\bar{4}3m$ point group symmetry the effective electrooptic constant behaves as

$$r_{eff} = r'_{333} \cos^2 \theta' + r'_{223} \sin^2 \theta'. \qquad (1.6)$$

This calculated dependence is shown in Figure 1.6. It is clear that going from the transmission geometry to reflection one we are changing not only the absolute value of r_{eff} but also its sign. In the experiment we observe the change in the direction of energy transfer in the beam coupling: the amplification of a signal wave changes to its depletion. The absolute values of the gain factor for the contrapropagated grating are plotted in Fig. 1.5 as diamonds ◆.

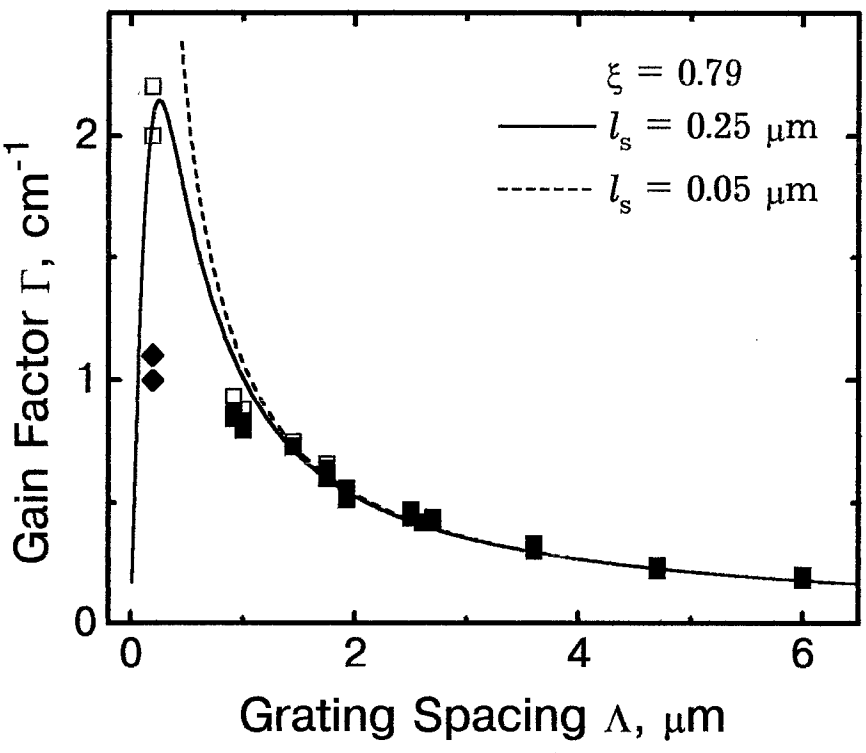

Fig. 1.5. Gain factor dependence on grating spacing.

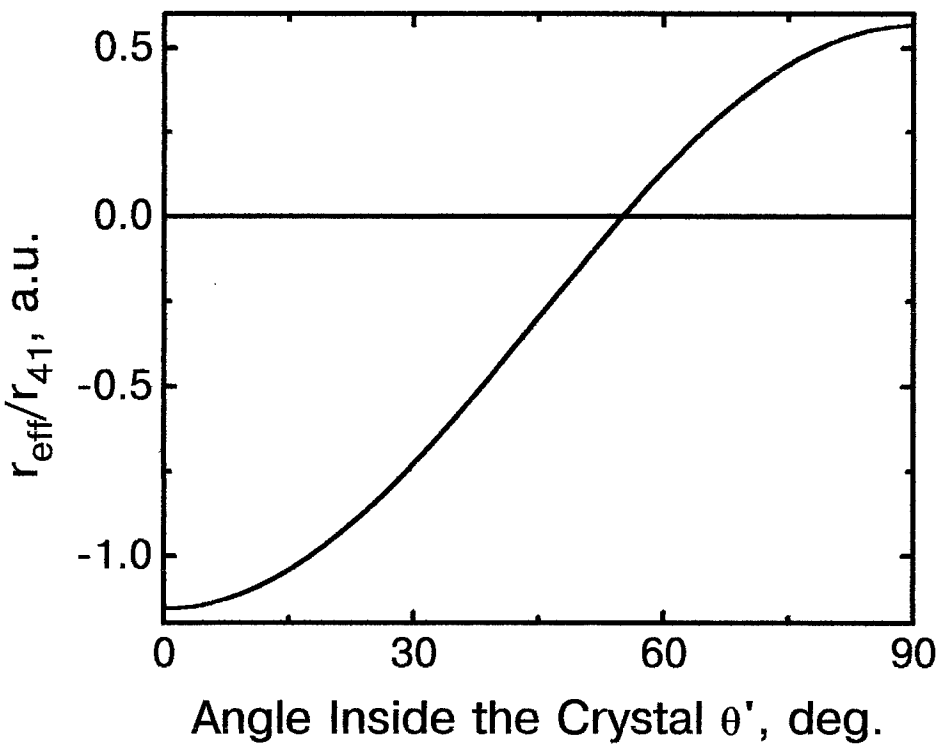

Fig. 1.6. Effective electrooptic constant as a function of pump angle θ' inside the crystal.

Thus to extract the value of Debye screening length from the grating-spacing dependence of the gain factor one should take into account the grating-spacing dependence of the effective electrooptic constant. To do it we renormalize the values of Γ for multiplying the measured values to r'_{333}/r_{eff}. The values which we get are plotted in Fig. 1.5 as open squares □. All following fits to theoretical dependences are done just with these data.

Note that the normalized gain factor for reflection geometry is two times larger then real experimental data because factor $r'_{333}/r_{eff} = r'_{333}/r'_{223} \approx 2$. This value of $\Gamma = 2...\ 2.2$ cm^{-1} correspond to those which could be measured for transmission gratings with spacing $\Lambda = 0.19$ μm (what is impossible at $\lambda = 1.064$ μm).

The solid line in Fig. 1.5 shows the theoretical fit (Eq. 1.4) with fitting parameters $l_S = 0.25$ μm and $\xi = 0.79$. When fitting we omitted the data for two smallest spacings with transmission geometry. These data correspond to largest intersection angles inside the sample which may result in artificial decreasing of the gain factor due to poor intersection of the recording beams.

With the estimate to Debye screening length we can evaluate the trap density from Eq. 1.5. With dielectric constant $\varepsilon = 10.3$ [1.15] we get $N_E = 9.2\times10^{15}$ cm^{-3}. This value is considerably larger then reported earlier for vanadium doped cadmium telluride, exceeding the data of Ref. 4 for vanadium concentration 1.6×10^{18} cm^{-3} ($N_E = 9\times10^{14}$ cm^{-3}) one order of magnitude and ≈ 2 times larger then the value in Ref. 6 for vanadium concentration 10^{19} - 10^{20} ($N_E = 4.3\times10^{15}$ cm^{-3}).

It should be noted that with germanium doped crystals we got the largest value of the gain factor $\Gamma = 1.1\ cm^{-1}$ as compared to any previously reported data with no electric field applied to the sample. Let us precise that with the available germanium-doped samples the use of optimum cut for the reflection geometry ($\vec{K} \parallel [001]$) should nearly double the gain factor and should permit the so called "net" amplification of weak signal beam incident to the crystal.

And nevertheless we are still far from the ultimate gain limited by the handbook values of electrooptic coefficient. We believe this is due to partial compensation of the main grating by antiphase grating of auxiliary carriers, i.e. because of $|\xi| < 1$. This give a certain hope that the gain factor can still be increased by technological means, e.g., by appropriate selection of dopants (codopants) and after-growth treatment (annealing).

1.4. Dynamics of grating recording and erasure in CdTe

The study of the kinetics of recording/erasure cycles in photorefractive material provides not only an information on characteristic relaxation times, important from the point of view of possible applications but permits also to evaluate some crystal parameters and compare them with independent measurements.

Figure 1.7a represents the temporal variation of the diffraction efficiency for recording/erasure cycle and Fig. 1.7b represents the logarithmic plot of diffracted beam intensity during the light-induced erasure of the grating. Both recording and erasure are monoexponential. As we are measuring the diffracted beam intensity, i.e., the value proportional to the second power of the light-induced refractive index change, to get the true value of time constant τ_{SC} one should multiply to 2 the grating decay time extracted from the slope of straight line in Fig. 1.7b. All data presented further on are corrected in such a manner.

The erasure of photorefractive hologram is caused by finite conductivity of the sample and the characteristic decay time is inversely proportional to the value of conductivity.

In addition the relaxation time is a function of Debye screening length l_S' and of the diffusion length L_D [1.17]:

$$\tau_{SC} = \frac{1 + K^2 L_D^2}{1 + K^2 l_S'^2} \times \tau_{di}, \qquad (1.6)$$

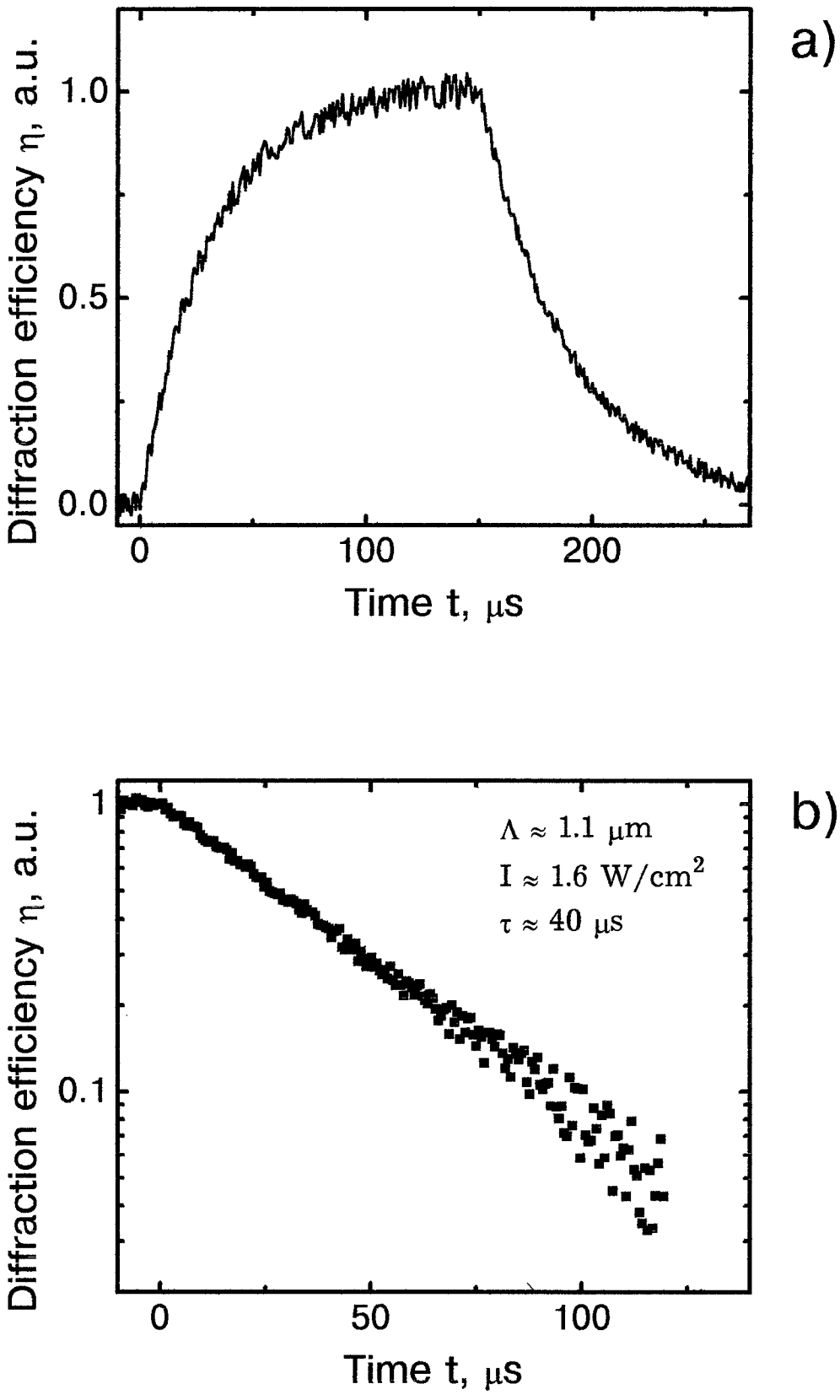

Fig. 1.7. (a) - diffraction efficiency of recording/erasure cycle;
(b) - logarithmic plot of light-induced erasure.

where K is the spatial frequency of the grating ($K = 2\pi/\Lambda$) and τ_{di} is the dielectric relaxation time:

$$\tau_{di} = \frac{\varepsilon\varepsilon_0}{\sigma_D + \kappa I}. \tag{1.7}$$

The diffusion length is introduced as

$$L_D = \sqrt{\mu\tau \frac{k_B T}{e}}. \tag{1.8}$$

In calculations and plots a value l_S' is used quite frequently which is related to Debye screening length by $2\pi l_S' = l_S$ or inverse value, $k_S = 1/l_S'$. Naturally, to determine the trap density one should now use:

$$l'_S = \sqrt{\frac{\varepsilon\varepsilon_0 k_B T}{e^2 N_E}}. \tag{1.9}$$

instead of Eq. 1.5.

This is done for the sake of easiness of presentation, to adjust the spatial frequency at which the maximum value of gain factor is reached to the inverse Debye screening length k_S.

We will use in what follows Eq. 1.6 rewritten as

$$\tau_{SC} = \frac{1 + K^2 L_D^2}{1 + K^2 (l_S / 2\pi)^2} \times \frac{\varepsilon\varepsilon_0}{\sigma_D + \kappa I}. \tag{1.10}$$

It is clear from Eq. 1.10 that the intensity dependence of the inverse relaxation time $1/\tau_{SC}$ should be linear.

For extremely low spatial frequencies the effect of limited transport length of photoexcited carriers is relatively small and the relaxation time of the space charge approaches the dielectric relaxation time. To determine this

time we measured the intensity dependences of the space-charge relaxation time for different spacings of the dynamic gratings (Fig. 1.8). The solid lines give the best fit to linear dependences.

With the grating spacing increasing to $\Lambda = 2.9$ μm the characteristic relaxation time becomes close to apparatus time of chopper Ch. The second factor limiting the use of larger fringe spacings is the decrease of the diffraction efficiency of the gratings recorded via diffusion charge transfer. Nevertheless with the data available we can estimate from the fit to Eq. 1.10 the lower limits for dark conductivity $\sigma_D \geq 1.5\times10^{-8}$ $(\text{Oh}\times\text{cm})^{-1}$ and for specific photoconductivity $\kappa \geq 3.7\times10^{-8}$ cm/B^2. These values are in agreement with the data for σ_D and κ extracted from the intensity dependence of the gain factor (see Chapter 1.2). The estimate for dielectric relaxation time τ_{di} with the data of Ch 1.2 and Eq. 1.7 provides dark relaxation time $\tau_D \approx 0.9$ ms or $\tau_{di} \approx 3$ μs for $I = 1$ W/cm^2.

The same grating-spacing dependence of relaxation time can be useful for evaluation of the diffusion length and Debye screening length. We can rewrite Eq. 1.10 in the form:

$$\frac{1}{I\tau_{SC}} = \left(\frac{\sigma_D}{I} + \kappa\right) \times \frac{1}{\varepsilon\varepsilon_0} \times \frac{1 + K^2\left(l_S / 2\pi\right)^2}{1 + K^2 L_D^2}. \qquad (1.11)$$

Equation 1.11 is valid when the K-dependent factor is the same for the dark- and photoconductivity, i.e., if the same carriers are responsible for dark- and photoconductivity. For the intensities where photoconductivity is much larger then the dark conductivity this expression defines the slope of the straight lines shown in Fig. 1.8. This approximation is well justified in our case

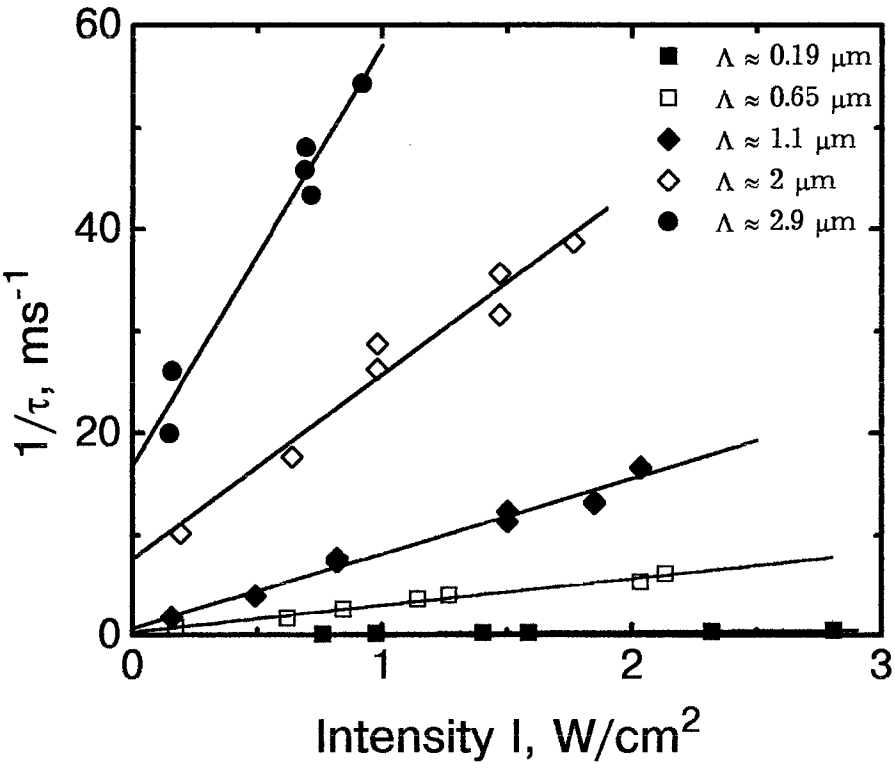

Fig. 1.8. Intensity dependence of inverse relaxation time.

because for 1 W/cm^2 the photoconductivity is 300 times larger then the dark conductivity according to the estimate of specific photoconductivity from the intensity dependence of the gain factor (and as minimum 7 times larger then the dark conductivity according to the estimate of specific photoconductivity from the intensity dependence of the grating relaxation time for fringe spacing equal to 2.9 μm).

Figure 1.9 represents (by dots) the dependence of the slope factor of the intensity dependences for reciprocal relaxation time versus spatial frequency. The measured data are within a certain interval of K; from the high spatial frequencies we are limited by spatial frequency of two counterpropagating waves, $K \leq 4\pi n/\lambda$, for sufficiently small spatial frequencies the relaxation time approaches to the apparatus time of the beam chopper. These limits prevent us from measurements of ultimate values of $1/I\tau_{sc}$ (for $K \rightarrow 0$ and $K \rightarrow \infty$) and characteristic points of inflection.

Even from this incomplete curve we are able to take some conclusions:

(*i*) Debye screening length is smaller then the diffusion length as the dependence of Fig. 1.9 is decreasing with the increasing of K (this property is common for all semiconductor photorefractives).

(*ii*) for small K the reciprocal grating relaxation time is equal to the dielectric relaxation time for intensity I = 1 W/cm . This means that this dielectric relaxation time is not longer then 24 μs and therefore the specific photoconductivity is not smaller then 3.7×10^{-8} cm/V^2 (the same estimate has been made already from the slope of the steepest dependence).

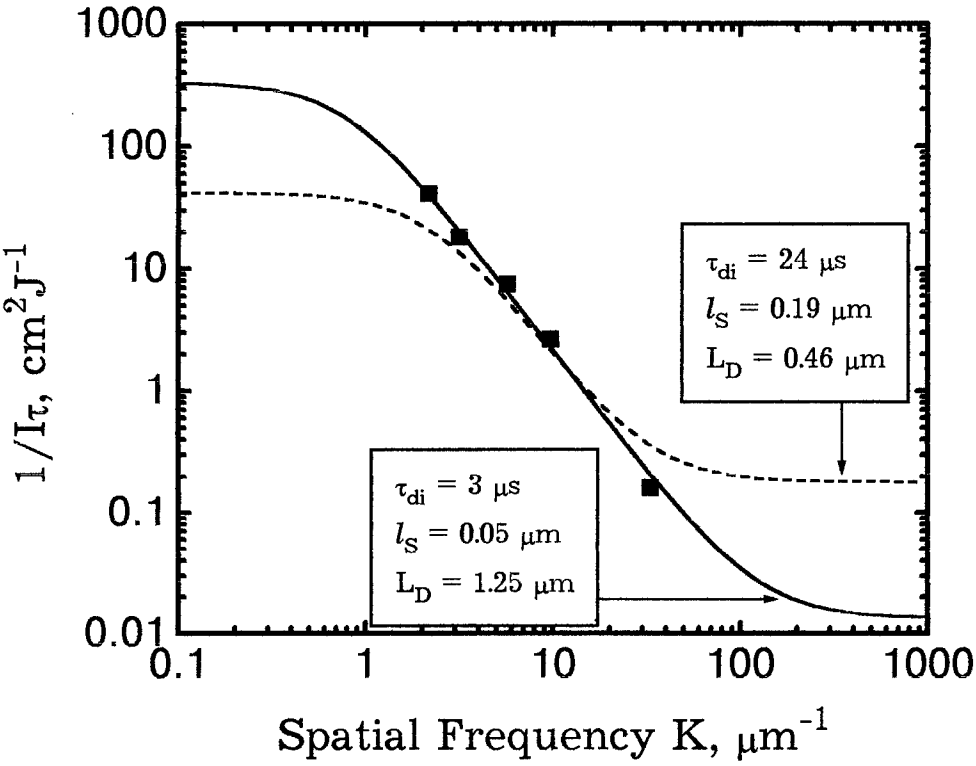

Fig. 1.9. Reciprocal product relaxation time x intensity as a function of spatial freguency ; experiment (squares); calculation from Eq. 1.11. (lines).

(*iii*) the rapid decrease of $1/\tau I$ corresponds to the spatial frequencies equal to the reciprocal diffusion length. Therefore the diffusion length is not smaller then 0.46 μm and the mobility-lifetime product is larger then 8.2×10^{-8} cm^2/V.

(*iv*) the decrease of $1/\tau I$ is completed at spatial frequencies larger then $2\pi/l_S$, therefore Debye screening length is smaller then the grating spacing for two counterpropagating light waves, i.e., $l_S < 0.19$ μm and $N_E > 1.6\times10^{16}$ cm^{-3} .

(*v*) for large K the value of $1/\tau I$ approaches the inverse dielectric time at I = 1 W/cm^2 multiplied by $(l_S/2\pi L_D)^2$.

The dashed line in Fig. 1.9 is calculated from Eq. 1.11 with the abovementioned limiting values of L_D, l_S and κ. The solid line in the same figure is a fit to Eq. 1.11 with the imposed parameter τ_{di} = 3 μs, evaluated earlier and the Debye screening length and diffusion length as free parameters. We extract from this fit l_S = 0.05 μm ($N_E = 2.3\times10^{17}$ cm^{-3}) and L_D = 1.25 μm ($\mu\tau = 6\times10^{-7}$ cm^2/V). Note that the fit becomes better for smaller Debye screening lengths.

The discrepancy of the data for Debye screening length evaluated in this Section and in Section 1.3 indicates to our opinion that the spatial frequency dependence of gain can hardly be used for correct estimates of crystal parameters, especially in case of several independent parameters involved. We show in Fig. 1.5 by dashed line the dependence calculated from Eq. 1.4 with l_S = 0.05 μm and the same ξ= 0.79. It is quite clear that the experimental data for extremely high spatial frequencies (reflection grating

geometry) are of largest importance. It should be underlined that these data are produced with the correction factors and therefore can have an additional scatter due to, e.g., imperfect orientation of crystallographic axes of the sample, etc.

The measured relaxation time (for optically and electrically isotropic cubic crystal) is independent of axis orientations and therefore it is not necessary to correct the values measured for different geometries. That is why we believe the data extracted from the measurements of time constants are more reliable.

The other reason for discrepancy is most probably connected to simultaneous presence of two types of charge carriers. The photon energy (1.17 eV) very close to the band gap (1.5 eV) and the estimated value of $|\xi| \neq 1$ suggest the simultaneous excitation of electrons and holes. Thus more complicated theory is necessary, taking into account contribution of complimentary charge carriers.

The hierarchy of different charge transport lengths for two types of carriers can strongly influence the formation of ultimate space-charge field; it can result even in inversion of beam-coupling direction when changing the spatial frequency of the recorded grating [1.18]. The strongest influence of this factor is at high spatial frequencies where it decreases the ultimate gain factor. Sometimes these decrease of the gain factor because of electron-hole competition at fringe spacings comparable to diffusion length can be misinterpreted as being due to trap saturation.

Taking into account all arguments mentioned above we come to conclusion that more plausible data for Debye screening length can be

extracted from spatial frequency dependence of the grating decay time as compared with the same dependence of the gain factor. This is especially true for our case with experimental data for different geometries of grating recording (transmission and reflection) and with Debye screening length out of the interval of measured spatial frequencies. Our estimate $l_S < 0.19$ μm and $N_E > 1.6\times10^{16}$ cm^{-3} seems to be reasonable because our CdTe samples have certainly larger density of dopant atoms (Ge) then this value of N_E.

REFERENCES TO SEC 1

1.1 M. B. Klein, Opt. Lett. **9**, 350 (1984).

1.2 USSR Invention Sertificat № 603276, Class G03H1/00, December 21, 1977, Published in Bull of Invention № 43, 250 (1978).

1.3 K. Tada and M. Aoki, Jpn. J. Appl. Phys. **10**, 998 (1971).

1.4 R. B. Bylsma, P. M. Bridenbaugh, D. H. Olson, and A. M. Glass, Appl. Phys. Lett. **51**, 889 (1987).

1.5 S. G. Odoulov, S. S. Slussarenko, and K. V. Shcherbin, Sov. Tech. Phys. Lett. **15**, 417 (1989).

1.6 M. B. Klein and G. C. Valley, J. Appl. Phys. **57**, 4901 (1985).

1.7 G. C. Valley, J. Appl. Phys. **59**, 3363 (1986).

1.8 F. P. Strohkendl, J. M. C. Jonathan, And R. W. Hellwarth, Opt. Lett. **11**, 312 (1986).

1.9 M. C. Bashaw, T.-P. Ma, and R. C. Barker, J.O.S.A. B **9**, 1666 (1992).

1.10 J. C. Launay, V. Mazoyer, M. Tapiero, J. P. Zeilinger, Z. Guellil, Ph.Delay, and G. Roosen, Appl. Phys. **A55**, 33 (1992).

1.11 V. V. Shepelevich and E. M. Hramovich, Sov.Phys.: Optic & Spectroscopy **85**, 403 (1986).

1.12 A. M. Glass and J. Strait, Photorefractive Materials and Their Applications I, edited by P. Gunter and J.-P. Hugnard, (Springer, Berlin) **61**, Chap. 8, p. 237 (1988).

1.13 N. V. Kukhtarev, V. B. Markov, S. G. Odoulov, M. S. Soskin, and V. L. Vinetskii, Ferroelectrics **22**, 949 (1979).

1.14 J. O. White, Sze-Keung Kwong, M. Cronin-Golomb, B. Fisher, and A. Yariv, Photorefractive Materials and Their Applications II, edited by P. Gunter and J.-P. Hugnard, (Springer, Berlin) **62**, Chap. 4, p.101 (1989).

1.15 A. J. Strauss, Rev., Phys., Appl. **12**, 167 (1977).

1.16 N. V. Kukhtarev, Sov. Tech. Phys. Lett. **2**, 438 (1976).

1.17 R. A. Mullen, Photorefractive Materials and Their Applications I, edited by P. Gunter and J.-P. Hugnard, (Springer, Berlin) **61**, Chap. 8, p. 167 (1988).

1.18 M. B. Klein and G. C. Valley, J. Appl. Phys. **57**, 4901 (1985).

2. BEAM-COUPLING IN SEMICONDUCTOR PHOTOREFRACTIVE CRYSTALS WITH MOVING GRATINGS

We study the possibility of evaluation of relaxation constants of semiinsulating photorefractive crystals like cadmium telluride and gallium arsenide from gain spectra of two-beam coupling. It is found that in many cases the shape of the measured spectra is different from the Lorentzian profile expected for monoexponential decay. Several possible reasons are analyzed to explain this behaviour. It is demonstrated also that in the case of bipolar conductivity and formation of two out-of-phase photorefractive gratings the ultimate gain factor can be increased by appropriate choice of the grating motion velocity.

2.1. Two-Beam-Coupling Spectra.

Photorefractive crystals allow for recording of "moving" gratings of the refractive index change by light waves with slightly different frequencies [2.1] and for amplification of shifted in frequency signal wave because of beam-coupling. The exponential gain factor for nondegenerate case is as follows (see, e.g., [2.2])

$$\Gamma = \Gamma_0 /(1 + \Delta\omega^2 t^2), \qquad (2.1)$$

where Γ_0 is the gain factor for strictly degenerate case i.e., for $\Delta\omega = 0$; $\Delta\omega$ is the frequency detuning and τ is the relaxation time of the grating.

We study experimentally the nearly degenerate interaction to determine the characteristic relaxation constants of semiinsulating photorefractive crystals like cadmium telluride and gallium arsenide. The gain factor is measured.

The experimental set-up is shown schematically in Fig. 2.1. An output the diode-pumped Nd^{3+}:YAG laser (TEM_{00}, λ =1.064 μm, beam waist ≈ 2 mm, output power up to 0.5 W) is splitted into two beams with the intensity ratio 1:100. The frequency detuning is introduced by two acousto-optic deflectors A1 and A2 which are put in both arms of interferometer. The deflector A1 introduces a constant detuning $\Omega_1/2\pi$ = 70 MHz wile deflector A2 introduces the tunable shift within the range from 40 MHz to 90 MHz (see Fig. 2.1). The accuracy of frequency adjustment $\Delta\omega/2\pi = (\Omega_1 - \Omega_2)/2\pi$ is not worse than 1 KHz, but it was impossible to adjust exactly the same frequency shift in both arms. The frequency shift necessary in the experiment does not exceed 200 KHz.

Figure 2.2 represents the experimental spectrum of the gain factor Γ (dots) measured for GaAs:Cr with the grating spacing $\Lambda \approx 0.87$ μm and total light intensity $I \approx 6$ W/cm^2. This dependence is well described by Eq. 2.1 (solid line) with fitting parameters $\Gamma_0 = 0.15$ cm^{-1} and $\tau = 100$ μs what is consistent with the directly measured values $\Gamma_0 \approx 0.15$ cm^{-1} and $\tau \approx 110$ μs for the same conditions.

For GaAs:Cr with larger grating spacing and for all possible grating spacings (from 0.19 μm to 3 μm) with CdTe:Cr the measured spectrum profiles differ considerably from the calculated.

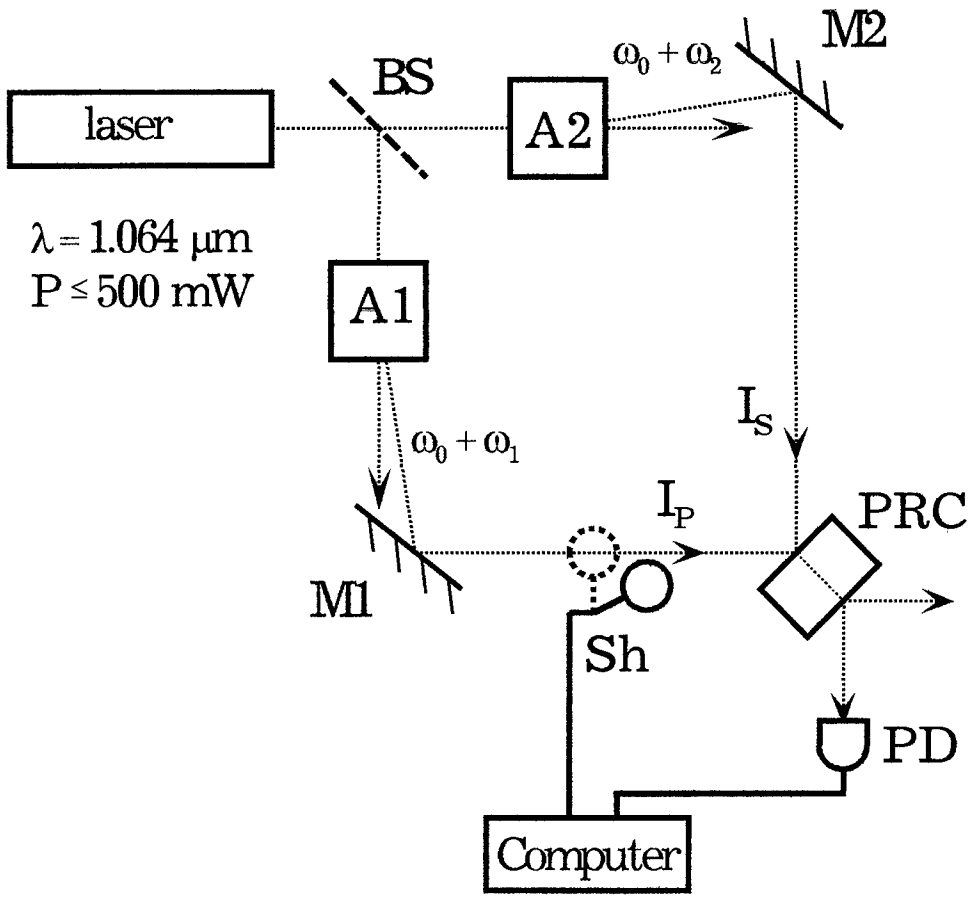

Fig. 2.1. Experimental set-up for moving gratings measurements. A1, A2 - acousto-optic deflectors.

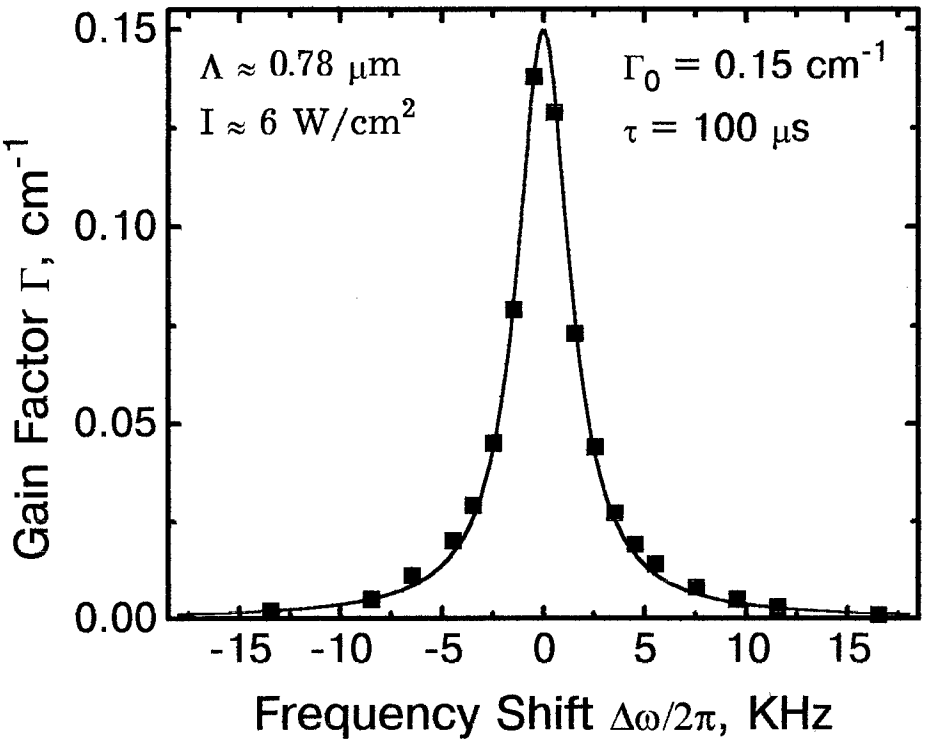

Fig. 2.2. Spectrum of the gain factor measured for GaAs:Cr; experiment (squares); calculation according Eq. 2.1 (line).

Figure 2.3 represents the experimental gain curve for the same sample of GaAs with grating spacing $\Lambda \approx 2.6$ μm and light intensity $I \approx 6$ W/cm^2. The calculation according to Eq. 2.1 with the independently measured $\Gamma_0 \approx 0.074$ cm^{-1} and $\tau \approx 12$ μs is shown by the solid line. The discrepancy of the measured and calculated spectrum is obvious.

The deviation from calculated gain profile is even more pronounced for cadmium telluride. The typical spectra for CdTe sample are shown in Fig. 2.4a,b for $\Lambda \approx 2.64$ μm and $I \approx 3.6$ W/cm^2 (a) and also for $\Lambda \approx 0.88$ μm and intensity $I \approx 5.1$ W/cm^2 (b). The calculated from the Eq. 2.1 dependences with the independently measured values of Γ_0 and τ (solid lines) are quite different from the measured. It should be underlined that sometimes the discrepancy of measured and calculated data looks different. Figure 2.5 represents the spectra for the reflection type gratings (counterpropagated pump and signal waves). It is very probable that points for strictly degenerate frequencies of two beams with exactly the same experimental conditions are missing in all curves.

2.2. Discussion

We consider in what follows the possible reasons for the observed discrepancy.

2.2.1. *Thickness-dependent relaxation time in absorbing crystals.*

The relaxation time of photorefractive grating is a function of the light intensity. For strong absorption and/or large interaction length the relaxation time is changing with the crystal thickness. Note that all intensities given in

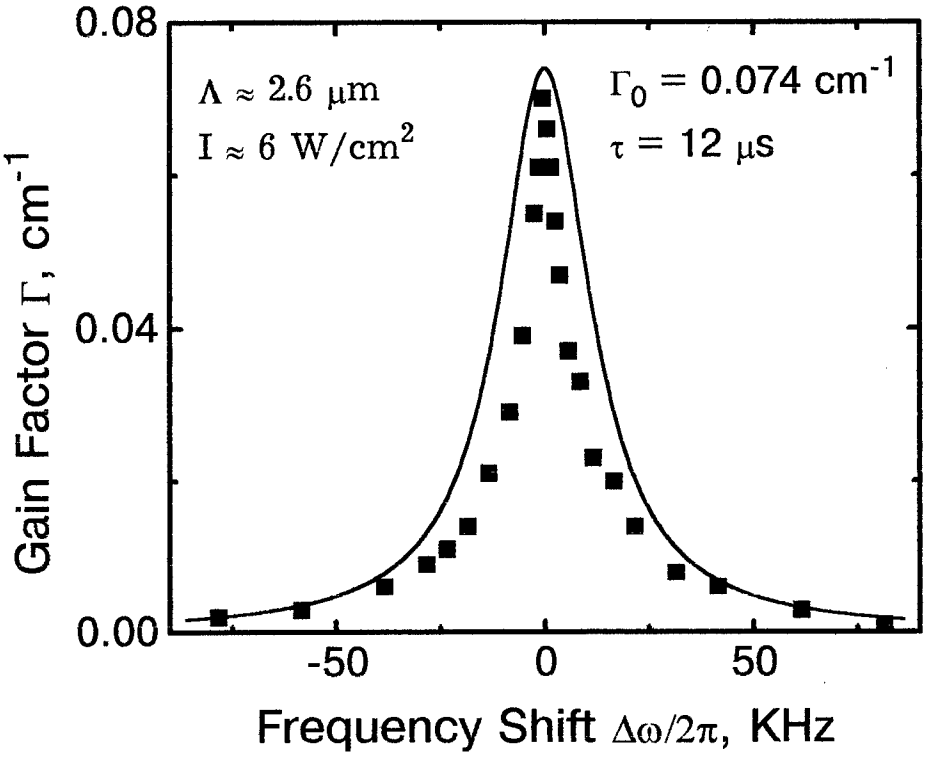

Fig. 2.3. Spectrum of the gain factor measured for GaAs:Cr; experiment (squares); calculation according Eq. 2.1 (line).

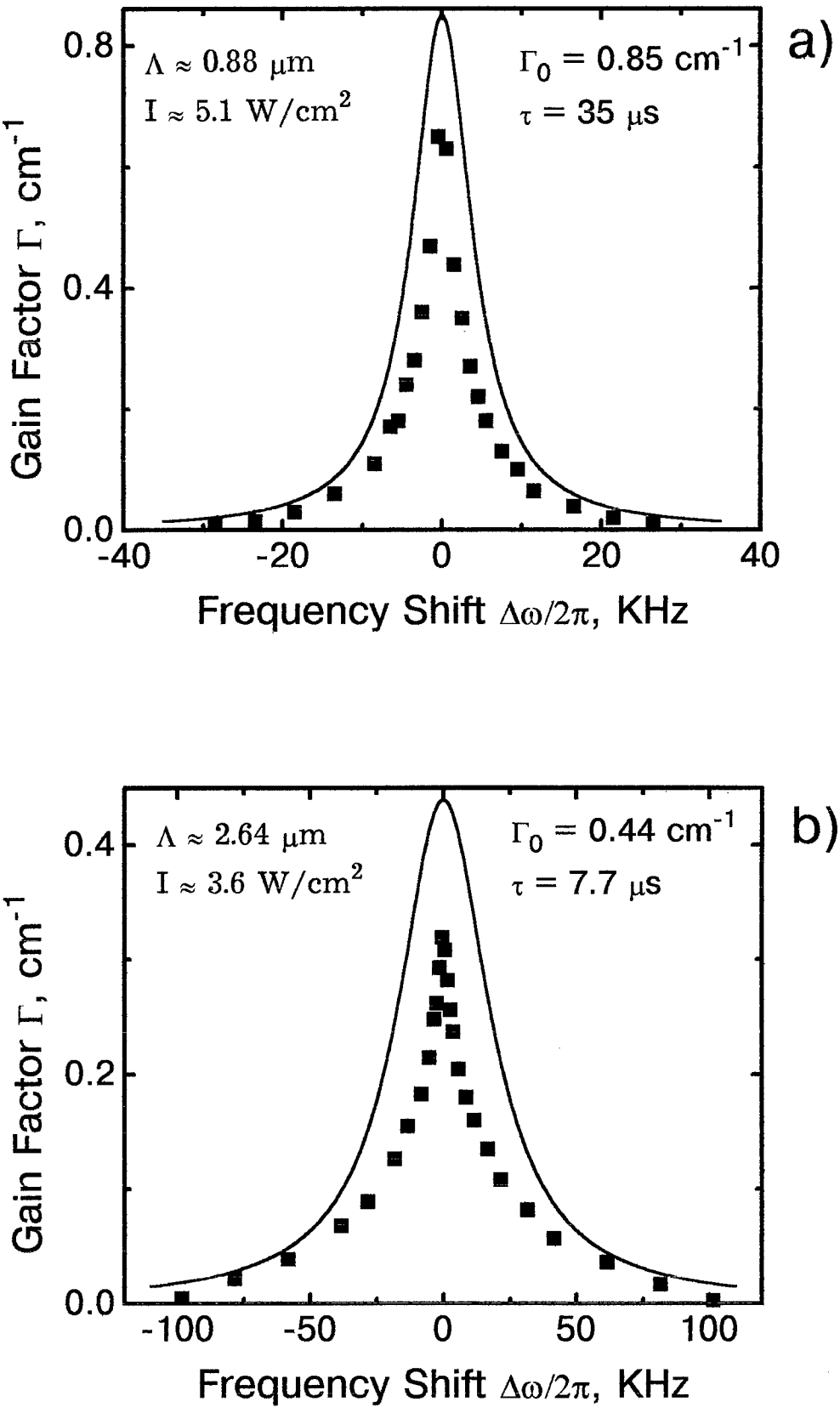

Fig. 2.4. Spectrum of the gain factor measured for CdTe:Ge
for differents grating spacings;
experiment (squares);
calculation according Eq. 2.1 (lines).

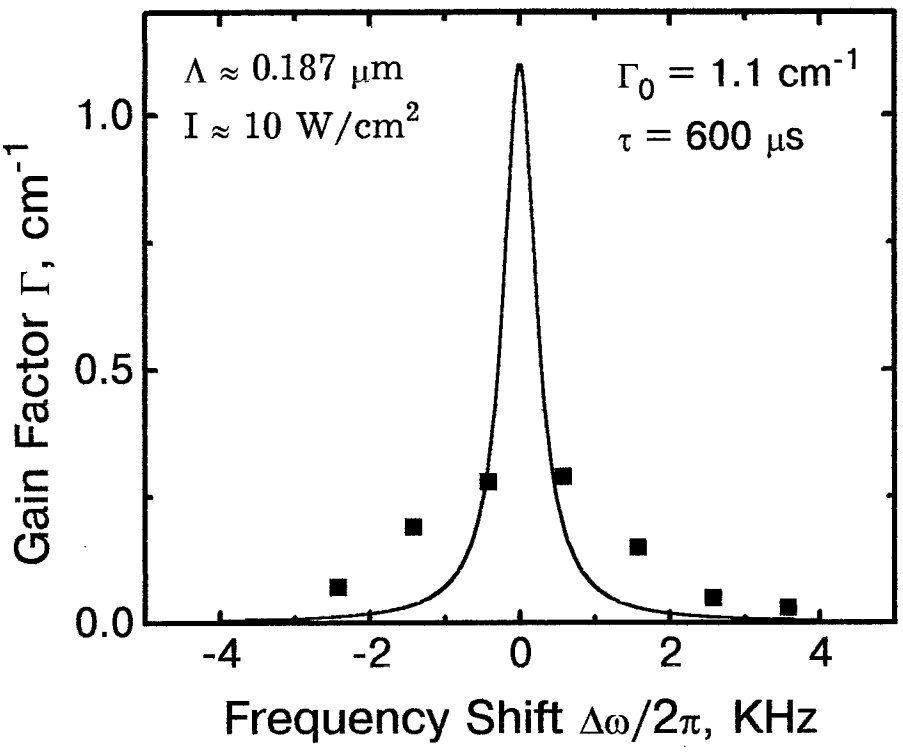

Fig. 2.5. Spectrum of the gain factor measured for CdTe:Ge
for reflection type of grating;
experiment (squares);
calculation according Eq. 2.1.

this report are integral intensities, i.e. thickness-averaged values. Thus the integral gain factor Γ for "moving" gratings should be thickness-averaged of elementary gain $\Gamma_i(x)$ and Eq. 2.1 should be rewritten as

$$\Gamma = \frac{1}{d}\int_0^d \frac{\Gamma_0(x)}{1+\Delta\omega^2\tau^2(x)}dx, \qquad (2.2)$$

where

$$\tau(x) \propto \frac{\varepsilon\varepsilon_0}{\sigma_D + \kappa I(x)}.$$

In our case the photoconductivity is much larger then the dark conductivity and therefore we can take Γ_0 = const and $\tau(x) \propto \frac{\varepsilon\varepsilon_0}{\kappa I(x)}$. Taking into account the variations of intensity as $I(x) = I_0\exp(-\alpha x)$ with the incident intensity I_0 we get instead of Eq. 2.1

$$\Gamma = \frac{\Gamma_0}{d}\int_0^d \frac{dx}{1+\Delta\omega^2\tau_0^2\exp(2\alpha x)}, \qquad (2.3)$$

with $\tau_0 \propto \frac{\varepsilon\varepsilon_0}{\kappa I_0}$.

After integration the final expression for gain spectrum becomes

$$\Gamma = \frac{\Gamma_0}{2\alpha d}\left[2\alpha d + \ln\left(1+\Delta\omega^2\tau_0^2\right) - \ln\left(1+\Delta\omega^2\tau_0^2\exp(2\alpha d)\right)\right]. \qquad (2.4)$$

Figure 2.6a,b shows the experimental data for CdTe with $\Lambda \approx 2.64$ μm and intensity $I \approx 3.6$ W/cm^2 (the same as in Fig. 2.4b). The thickness of this sample is $d \approx 0.65$ cm and its absorptivity $\alpha \approx 1.2$ cm^{-1}. The solid line in Fig. 2.6 a shows the results of calculation according to Eq. 4 with $\tau_0 = 7.7$ μs and $\Gamma_0 = 0.44$ cm^{-1}.

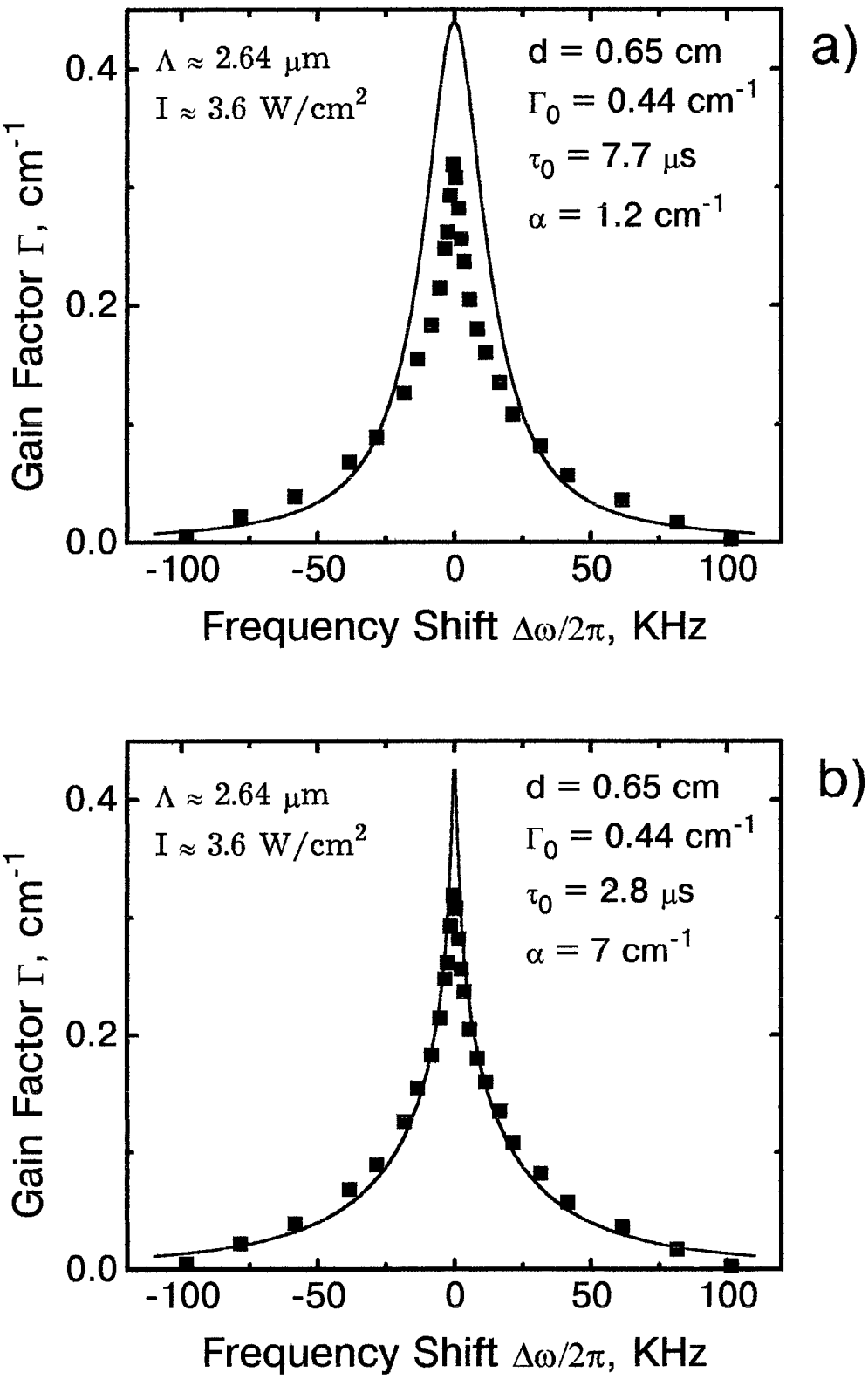

Fig. 2.6. Spectrum of the gain factor measured for CdTe:Ge;
experiment (squares);
calculation absorbtion taking into account (lines):
(a) - with real value of $\alpha = 1.2\ cm^{-1}$,
(b) - best fit gives $\alpha = 7\ cm^{-1}$.

Figure 2.6 b represents the best fit with d = 0.65 cm, Γ_0 =0.44 cm^{-1} and fitting parameters τ_0 and α. From this fit we get $\alpha \approx 7$ cm^{-1} and $\tau \approx 2.8$ μs.

Thus the shape of the experimental curve can be satisfactory described by Eq. 2.4 but for obviously unrealistic values of α and τ_0. This lead to conclusion that the other reason for particular shape of the gain spectrum exists apart from (or in addition to) the nonuniform intensity distribution in the crystal thickness.

2.2.2. *Complicated spectra because of the recording of several gratings with different lifetimes.*

If we suppose the existence of two independent gratings with different characteristic relaxation times τ_1 and τ_2 we can wait for the gain spectrum consisting of two superposed Lorentzian profiles

$$\Gamma = [\Gamma_1 /(1 + \Delta\omega^2\tau_1^2)] + [\Gamma_2 /(1 + \Delta\omega^2\tau_2^2)], \qquad (2.5)$$

where Γ_1 and Γ_2 are zero values of gain factor for two components. The sum $\Gamma_1 + \Gamma_2$ should be equal to Γ_0.

Figure 2.7 represents the results of the fit of the spectrum for CdTe with $\Lambda \approx 2.64$ μm and $I \approx 3.6$ W/cm^2 (the same as given by Fig. 2.4b).

One can see that this fit looks reasonable. The direct measurements of the decay of the diffracted beam intensity do not reveal two- or multy-exponential kinetics (see Fig. 1.7). Thus the described attempt to explain the unusual shape of the gain spectra by two-component-grating must be supported by use of more complicated model. Perhaps the secondary centers manifest

themselves [2.4,2.5] in gain factor spectra but not in direct measured relaxation proces.

2.3. Enchancement of beam-coupling by grating motion

By using the moving grating technique, without an applied electric field, it is possible to increase the steady-state two-beam coupling gain in photorefractive $Sn_2P_2S_6$.

Tin hypotiodiphosphate ($Sn_2P_2S_6$, SPS) was shown to be promising photo-refractive material for near infrared region of spectrum with relatively high transient gain factor (up to 6 cm^{-1}) and rather short response time of transient peak (10^{-1} to 10^{-2} s) [2.6]. The steady-state gain factor which is established after approximately 10^3 s is usually much smaller, reaching approximately 1 cm^{-1}. We show in what follows that with small frequency detuning of one of two writing beams the steady-state gain can be achieved close to the peak value of the transient gain for strict frequency degeneracy.

SPS is a monoclinic ferroelectric crystal which belongs to the P_c symmetry class [2.7,2.8]. The samples are reddish-brownish in color. They strongly absorb the green radiation from the Ar^+-laser or second harmonic of a Nd^{3+}:YAG laser, but are transparent for 632nm and longer wavelengths. The photorefractive grating recording via diffusion charge transport was reported for this material at λ = 0.6328 μm [2.9,2.10] and at λ = 1.064 μm [2.6]. To record a grating two light waves are directed to the sample in plane normal to the OY axis in such a way that grating vector is parallel to the OX axis [2.11], i.e., nearly parallel to the axis of spontaneous polarization. Both beams are identically polarized with the electric field vector in the plane of incidence.

In our experiments the single-mode, single-frequency 1.06 μm radiation of a diode-pumped Nd^{3+}:YAG laser with an output beam power of 600 mW

is used for the grating recording. A schematic representation of the experimental set-up is shown in Fig. 2.8. The unexpanded light beam from the laser passes through a $\lambda/2$ phase retarder and polarizer to obtain horizontal polarization. The beam splitter BS forms two beams, with the strong pump wave directed to an electrooptic modulator and then to the SPS sample. The weak signal beam, attenuated by neutral density filter ND, also is dirtected to the SPS sample. The angle between two beams is chosen 60° to assure the grating spacing $\Lambda = 1\mu m$. The intensity of the output signal beam is continuously monitored by the detector D and digital oscilloscope.

The electrooptic modulator is driven with a periodic saw-tooth signal. The amplitude of modulation is adjusted to provide exactly a 2π phase shift in the pump wave during one period; the frequency of modulation can be changed. In this way, the linear in time modulation of phase is introduced in the pump wave, which is equivalent to a frequency shift of the pump wave with respect to the signal wave.

The single-frequency Nd^{3+} : YAG laser assures a large coherence length of output radiation, that is why we were able to use an asymmetric scheme of recording with different lengths of the two arms of the interferometer (Fig. 2.8). In fact the other reason to use it is connected with the relatively high divergence of the laser beam: with the longer arm of the pump wave, the diameter of the pump beam is larger than the signal beam at the sample. The measured 1/e beam waists on the crystal were 1.7 and 0.93 mm for the pump and signal beams, respectively. Thus the intensities of the pump and signal

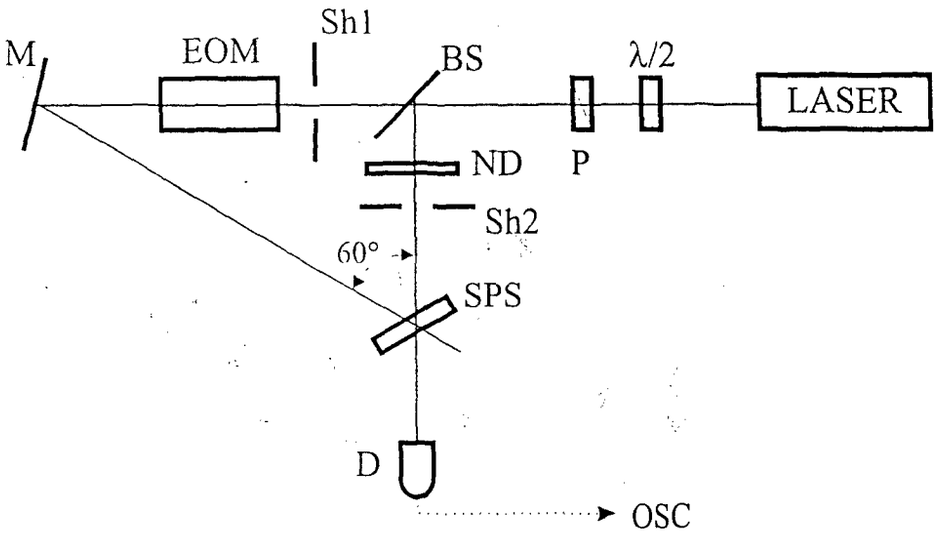

Fig. 2.8. Experimental set-up.

beams on the input face of the sample were 15 W/cm^2 and 43 mW/cm^2, respectively.

The crystals of $Sn_2P_2S_6$ studied in this work were grown in Institute of Solid State Physics and Chemistry, Uzhgorod State University, 294000 Uzhgorod, Ukraine. Typical sample sizes are 5x5x1.2 mm^3 along X, Y, and Z axes. To increase the sensitivity of the crystal to infrared light it was illuminated by incoherent white light (100W- halogen lamp at 5 cm distance from the sample, exposure time 30 min). Once illuminated, the sample remains sensitive for a minimum of one day. Consecutive write-erasure cycles with infrared light do not change, in first approximation, the sensitivity to subsequent recording.

With this set-up we measure first the dynamics of the beam coupling for the strictly degenerate case at ambient temperature 20°C (Fig. 2.9). The results agree qualitatively with that reported in [2.6]. When the pump wave is switched on the intensity of the weak signal wave increases quickly, reaching a certain peak value and then decreases with a much slower rate. The steady-state is established after 10^3 seconds. This type of dynamics suggested the model of two movable species of charge carriers, with simultaneous excitation resulting in partial compensation of a grating in steady-state (see, e.g., Ref. 2. 14). The independence of the slow response time to light intensity leads to the conclusion that the slow grating is formed by thermally excited carriers [2.6].

One can expect that the recording of this slow grating can be eliminated by proper choice of frequency shift in the moving grating technique. If the frequency detuning is larger than the reciprocal relaxation

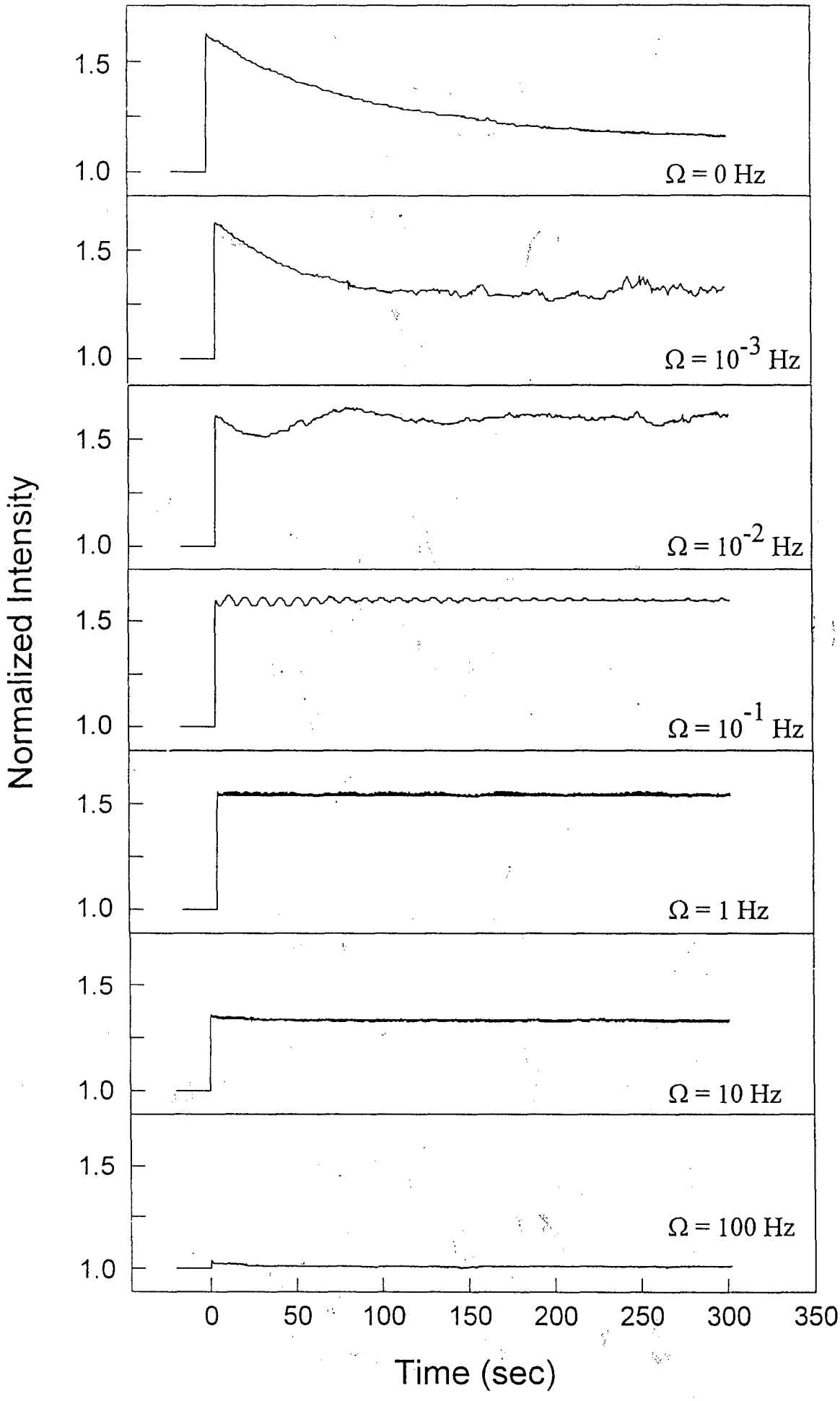

Fig. 2.9. Dynamics of weak beam intensity in beam-coupling experiment.

time for the slow component, but still much smaller than that for fast component, it should be possible to reach the steady-state gain factor close to its transient peak value in frequency degenerate case. For diffusion dominated charge transport, i.e., for a $\pi/2$ shifted phase grating, the result of interaction must be insensitive to the direction of grating motion, i.e., to the sign of the frequency shift. The second advantage, as it will become clear from what follows is considerable reduction of the relaxation time of the signal amplification.

Fig. 2.9 shows the temporal variation of the signal beam intensity for different values of frequency detuning Ω. It is quite clear from these data that for W less than 1Hz the peak value of gain is the same for all these curves while the steady-state value of gain is gradually increasing when Ω becomes larger. This is in complete agreement with our expectations. For larger frequency detuning, e.g., for Ω = 10 or 100 Hz, the transient peak is no longer visible, but the saturation value of gain becomes smaller than at low frequencies. This decrease of intensity is a consequence of the grating moving too fast compared to $1/\tau_f K$, where τ_f is the relaxation time of the fast component and K is the spatial frequency of the grating.

We measured the dependence of the gain factor on frequency detuning (Fig. 2.10). The gain factor Γ is introduced in the usual way as $\Gamma = (1/d)\ln[I_s/I_s^o]$, where d is the sample thickness, I_s and I_s^o are the intensities of the output signal wave in presence and with no pump wave, respectively. Two values are given for any particular frequency detuning Ω , one for transient gain (I_s stands for the peak value of intensity after onset of the pump wave)

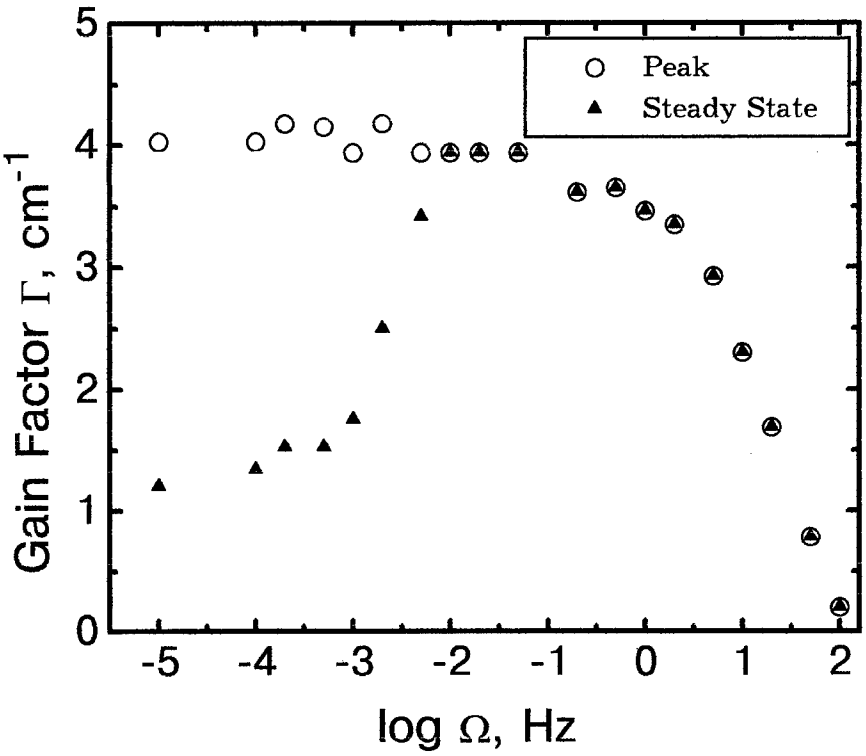

Fig. 2.10. Frequency dependence of the gain factor.

and other for steady-state gain (I_s stands for saturated value of weak beam intensity). The logarithmic scale is chosen for Ω to clearly show the frequency dependence of the steady state gain at low modulation frequencies. This kind of plot does not permit showing the response for negative values of frequency detuning. It should be emphasized, however, that within experimental error the measured values for $+\Omega$ and $-\Omega$ are the same.

It is clear from Fig. 2.10 that with the pump intensity of 15 W/cm^2 one can use SPS within the range of frequency detuning (0.005 to 1Hz) with loss of gain of no more than 15 %. The characteristic relaxation times (estimated from frequency detuning necessary to change the ultimate gain factor two times) are τ_f = 70 ms and τ_s = 500 s for fast and slow components, respectively. It should be noted that the grating decay is not exponential and therefore the profile of gain spectra is not Lorentzian; so the presented data for τ_f and τ_s can not be considered as the standard 1/e decay times.

As can be seen from Fig. 2.9, the intensity of the amplified signal beam is periodi-cally modulated with the frequency equal to frequency shift between two waves, Ω. Figure 2.11 represents the dependence of deviation from the mean value of gain factor (given in Fig. 2.9) as a function of frequency detuning. For the worse situation, at Ω = 0.005 Hz the largest deviation $\Delta\Gamma/\Gamma$ does not exceed 0.17. Note that even in this case the mean value of Γ is established within 100 ms, i.e., much faster then the steady-state gain for waves with the same frequency.

The unusual shape of the gain frequency spectra for SPS crystals can be used to build a simple Novelty Bandpass Filter [2.13] which is able to select

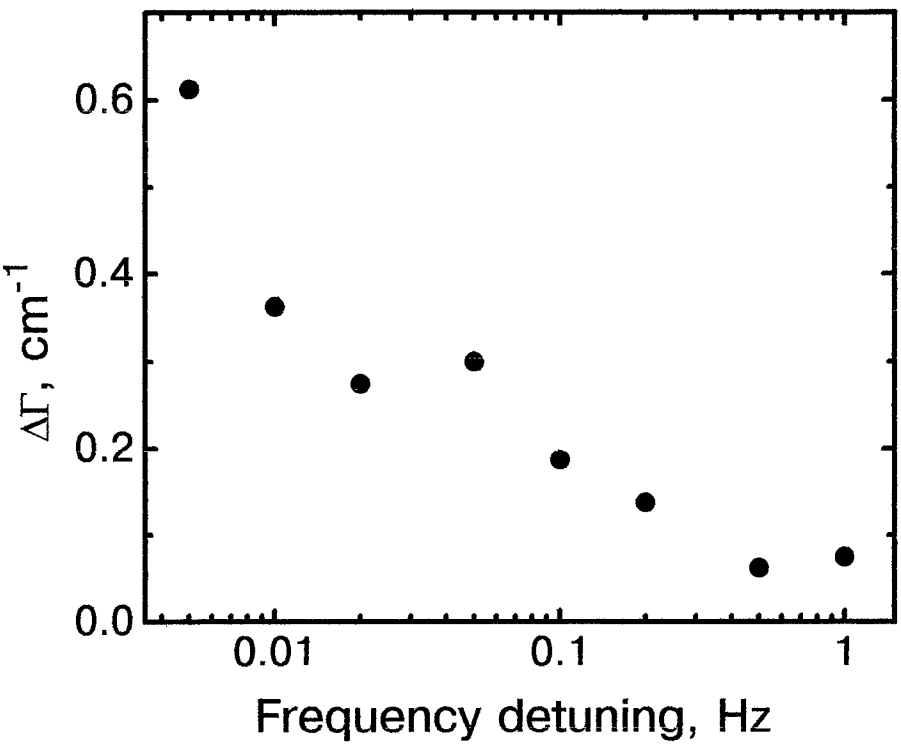

Fig. 2.11. Amplitude of temporal variations of the gain factor versus frequency detuning

the objects moving within a certain speed interval. For a 0.8 cm thick sample with the gain factors given in Figure 2.10 an object moving with the optimum speed will be exp(3-1) times brighter than immobile objects or objects moving with too much speed. This contrast can be further improved with the ultimate values for gain factor $\Gamma \approx 6.5\ cm^{-1}$ reported in [2.6].

REFERENCES TO SEC 2

2.1 S. I. Stepanov, V. V. Kulikov, M. P. Petrov, Opt. Comm. **44**, 19 (1982).

2.2 J. Feinberg, D. Heimann, A. R. Tanguay, Jr. and R. W. Hellwarth, J. Appl. Phys. **51**, 1297 (1980).

2.3 K. Walsh, A. K. Powell, C. Stace, and T. J. Hall, JOSA B **7**, 288 (1990).

2.4 G. A. Brost, R. A. Motes, and J. T. Rotge, JOSA B, **5**, 1879 (1988).

2.5 L. Holtman, Phys. Stat. Sol. (a) **113**, K89 (1989).

2.6 A. Shumelyuk, U. Hellwig, R. Rupp, S. Odoulov, and A. Grabar, in Technical Digest of Topical Meeting "Photorefractive Materials, Effects, and Devices. PR`95" Aspen Lodge, Colorado, June 1995, pp.80-84. [also submilled to JOSA B Feature Issue on Photorefractive Materials].

2.7 C. D. Carpentier and R. Nitsche, Material Res. Bull. **9**, 1097 (1974).

2.8 G. Dittmar and H.Schaefer, Z. Naturforschung, **29b**, 312-317 (1974).

2.9 A. A. Grabar, R. I. Muzhikash, A.D. Kostiuk and Yu. M. Vysochanskii, Sov. Physics, Solid State **33**, 1314-1316 (1991).

2.10 A. A. Grabar, Yu. M. Vysochanskii, I. M. Stoyka, M. M. Dan'ko, and V. Yu. Slivka, Ukrainian Physical Journal **39**, 941-942 (1994).

2.11 We adopt and use the following notations for crystal axe [3]: axis OY is normal to the unique plane of symmetry of the crystal, axis OX is nearly parallel to the axis of spontaneous polarization.

2.12 S. Zivkova and M. Miteva, J. Appl. Phys. **68**, 3099-3103 (1990).

2.13 D. Z. Anderson and J. Feinberg, IEEE J. Quantum Electron. **25**, 635 (1986).

3. BEAM-COUPLING IN CdTe WITH EXTERNAL ELECTRIC FIELD

It is known that the efficiency of the beam-coupling can be improved several times by application of the external electric field [3.1]. Of great importance in this connection is not only the amplitude of the electric field but also the shape of its modulation [3.1,3.2]. The best known for today is the symmetric rectangular shape with alternating sign (square shaped AC field). It is necessary to chose the temporal period of the modulation which is larger then the lifetime of the free carriers but smaller then dielectric relaxation time of the crystal.

This is relatively easy to meet this requirements to improve the beam-coupling in slow-response sillenite-type crystals and to assure the high-quality square-shaped modulation of the field. It is much more difficult to do when applying this technique to semiconductor crystals with short response times. That is why a problem of optimization of all parameters of interaction is especially hard for semiconductor photorefractives with an external AC field.

3.1. Beam-coupling with high-frequency sinusoidal electric field.

To check the possibility of improvement of photorefractive properties of the available CdTe crystals we start with application of the high frequensy sinusoidal external voltage with. A special power supply was designed with 18 KHz modulation frequency and the amplitude assuring the field up to 6 KV/cm. Note, that as in all previous publications on semiconductor

photorefractives with AC field [3.3-3.5] we are using sufficiently large modulation frequency.

The silver paint electrodes were deposited to the sample faces parallel to (111) planes; with these electrodes the voltage was applied along the grating vector $\vec{K} \parallel [111]$. The effect of field on beam coupling gain factor was measured. Figure 3.1 shows (by dots) the measured dependences of the gain factor on grating spacing for two values of the applied field ≈ 3.1 KV/cm and ≈ 6 KV/cm. It is obvious that the use of this AC-field supply with the amplitude voltage on the sample nearly 6 KV/cm resulted in nearly three-times increase of the gain factor at optimum grating spacing for transmission geometry: from $\Gamma \approx 0.85$ cm^{-1} at $\Lambda_{opt} \approx 0.9$ μm without any applied field to $\Gamma \approx 2.1$ cm^{-1} at $\Lambda_{opt} \approx 20$ μm with external sinusoidal electric field.

When performing these preliminary tests we discovered some extra experimental difficulties. If with the applied high voltage the resistivity of the illuminated area is droping down 10^8 Ohm×cm the sample starts to be heated by the electric current. This increase of temperature, in turn, leads to the decrease of resistivity and therefore to further increase of current density. The highest intensity which is still below the threshold of thermal breakdown is by itself a function of the applied field amplitude. To avoid the damage of the unique sample it was necessary to restrict ourselves by the small intensities and to keep crystal with the applied voltage only during relatively short time (usually few seconds, below 10 s).

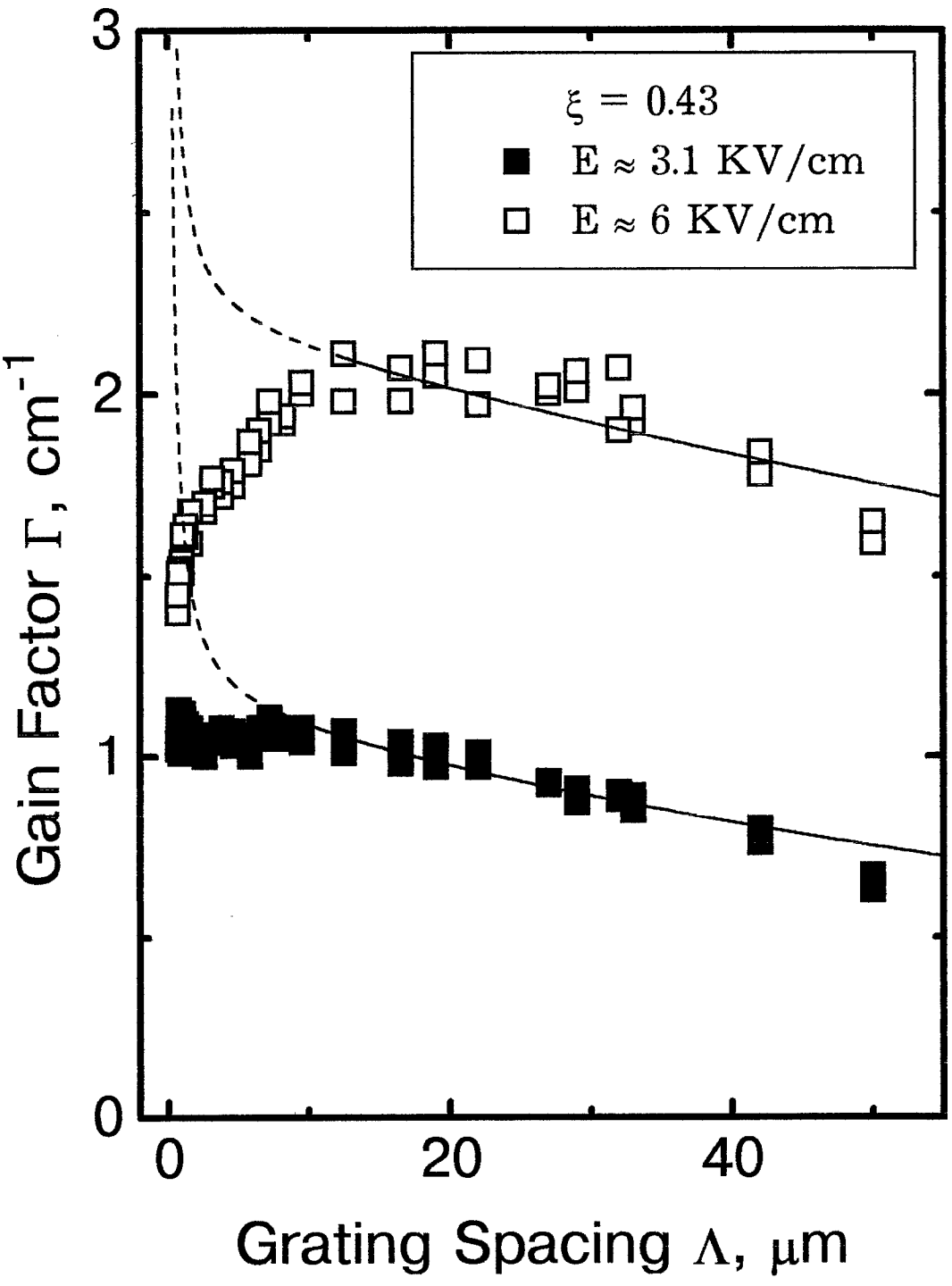

Fig. 3.1. Gain factor as a function of grating spacing with external sine electric field.

3.2. Beam-coupling with low-frequency sinusoidal and square-shaped electric field.

Let us consider the necessity of application just of high-frequency AC field to improve the photorefractive properties of semiconductor photorefractive crystals. In presence of external electric field Eq. 2.6 should be modified in a following manner

$$\tau_{SC} = \frac{\left(1 + K^2 L_D^2\right)^2 + K^2 L_E^2}{\left(1 + K^2 L_D^2\right)\left(1 + K^2 l_S'^2\right) + K^2 L_E l_E} \times \tau_{di}, \qquad (3.1)$$

where $l_E = \frac{\varepsilon\varepsilon_0 E}{eN_E}$ is the length of carrier tightening by the electric field E, and

$L_E = \mu\tau E$ is the carrier drift length.

It follows from Eq. 3.1 that apart from the increase of the grating relaxation time with the increasing spatial frequency K the additional slowing-down of the relaxation occurs due to the external applied field.

The factor in Eq. 3.1 before dielectric relaxation time is equal to 10^4 for the sample tested in case of square-waveform electric field applied with amplitude of 10 KV/cm. Taking into account nonzero dark conductivity and intensity dependence of the gain factor (see Fig. 1.4) one should use the input beam intensity not less then 30 mW/cm^2 to assure an effective recording. The dielectric relaxation time evaluated from Eq. 1.7 with the known dark conductivity and specific photoconductivity appears to be 85 μs. In the same time the grating relaxation time in applied field comes close to 1 second. Therefore the use of very high modulation frequency is not indispensable.

Moreover, with very small Debye screening length as it is in this sample we can not expect the high-frequency fall-off in the dependence of the space-charge amplitude on grating spacing and.

This is why we continue our experiments with the square-shaped AC field with more moderate frequencies within the interval (0.03.... 4) KHz. In all experiments we measure in addition the response to the sinusoidal AC field as a reference. The power supply was built with Synthesized Function Generator Stanford Research Systems Model DS345 and High Voltage Trak Amplifier Model 609C-6.

As the perfect shape of AC field modulation is a crucial point for formation of ultimate space-charge [3.2] we first checked the quality of output signal of an amplifier. The shape of modulation in output signal can be represented in first approximation as a Slew-Rate-Limited Square Waveform (Fig. 3.2). With the increasing of modulation frequency from 100 Hz to 2.5 KHz the pulse front parameter R is increasing from 0.015 to 0.33.

To define the best experimental parameters assuring the largest possible gain we measure the gain factor as a function of grating spacing for different light intensities. The amplitude of the applied field is about 8.8 KV/cm both for square-shaped and for sinusoidal modulation. The beam intensity ratio was kept $\beta \approx 1{:}300$. For small spatial frequencies we were restricted in our choice of beam ratio by light scattered from optical imperfections of the sample in direction of the signal wave from the pump wave. The change of total light intensity had two aims: to determine the intensity wich is small enough for particular grating spacing and assures sufficiently long dielectric relaxation

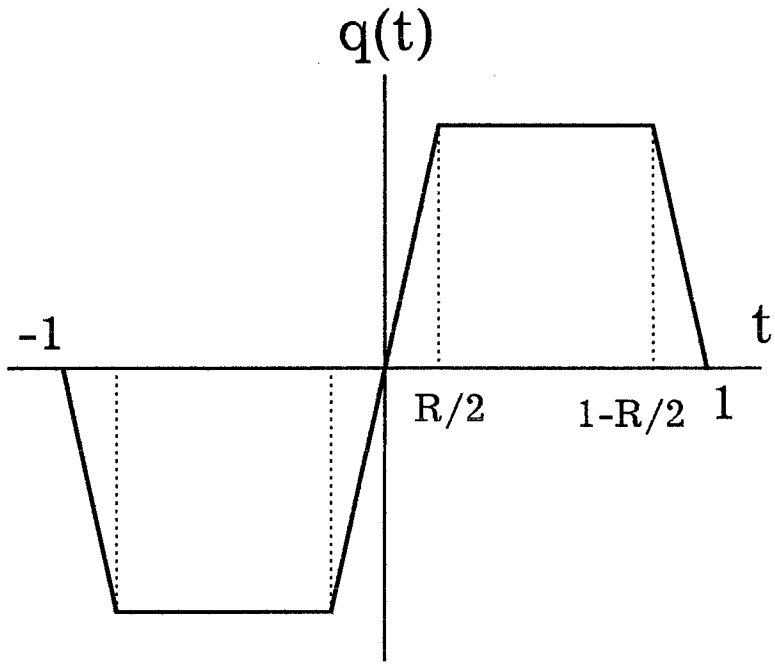

Fig.3.2. Slew-rate-limited square waveform.

time and, in the same time, large enough to record the efficient grating. The results obtained for grating spacings 2.8, 4.4, 8, 14, 19.3, and 30 μm are shown in Figures 3.3 a-l, respectively.

With the increasing modulation frequency the gain factor is rapidly growing for square-shaped as well as for sinusoidal modulation of an applied voltage. With increasing intensity and grating spacing as one could expect this growth becomes more slow. For square-shaped modulation the gain factor reaches a maximum value at a certain modulation frequency and is decreasing with increasing further frequency. In the same time for sinusoidal modulation the gain factor saturates after reaching its largest value. This comparison suggests the explanation of the decreasing gain factor by increasing deviation from perfect square-shape when modulation frequency becomes larger.

Now we describe our attempt to take into account (evaluate) the possible effect of the imperfect shape of modulation on the space-charge field [3.2]. With the AC field applied its effect can be described by a factor η which is introduced as a ratio of gain factor in AC field to that in DC field with the same amplitude:

$$\eta = \frac{1}{I_0(P)} - \frac{1}{P}, \tag{3.2}$$

where P depends only on material parameters L_E and L_D and on spatial frequency K:

$$P = \frac{L_E K}{1 + L_D^2 K^2}, \tag{3.3}$$

$I_0(P)$ is the integral taking into account the evolution of physical parameters during one period of variation of the applied field:

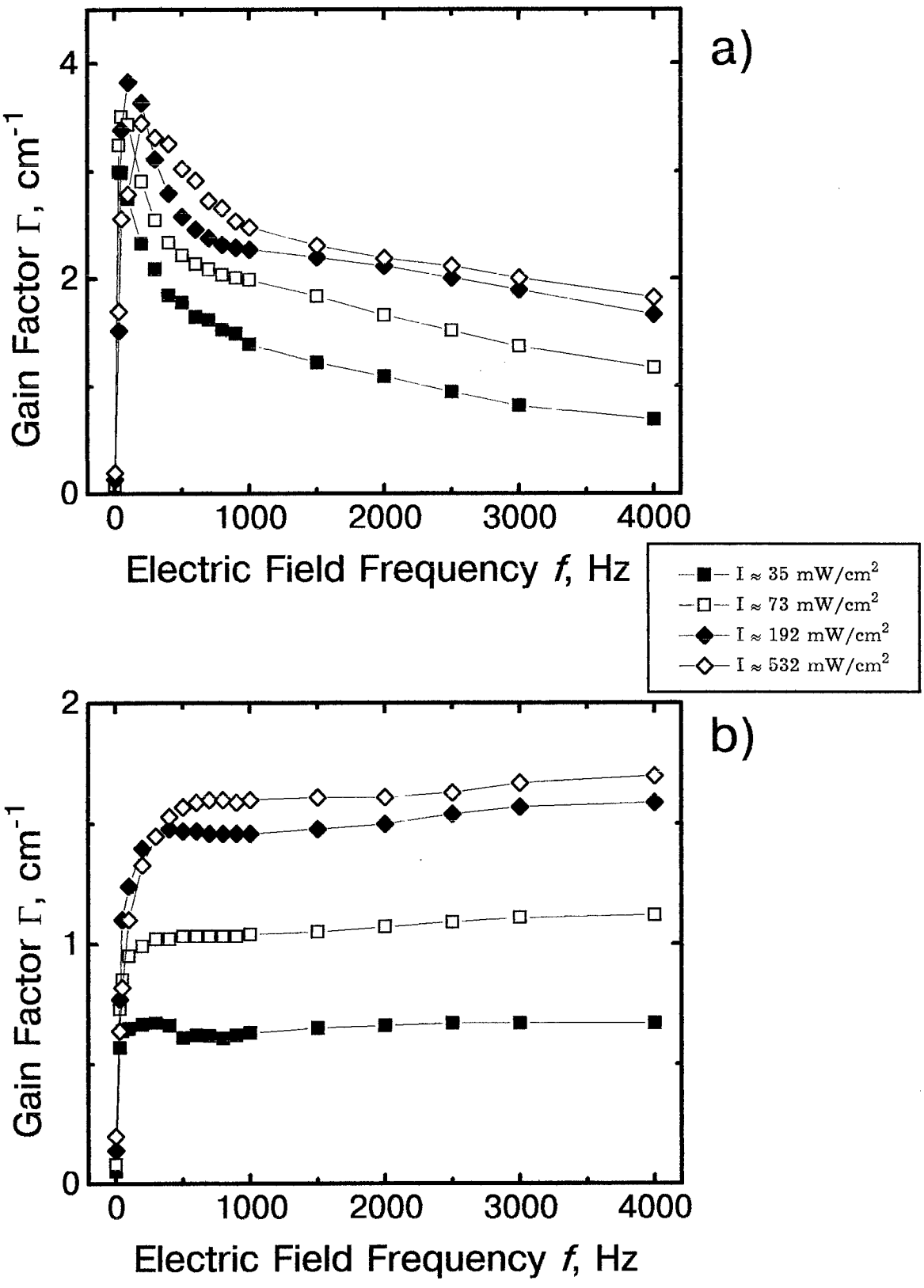

Fig. 3.3. Gain factor as a function of applied field frequency for Λ = 2.8 μm and for different intensities;
(a) - slew-rate waveform;
(b) - sine waveform.

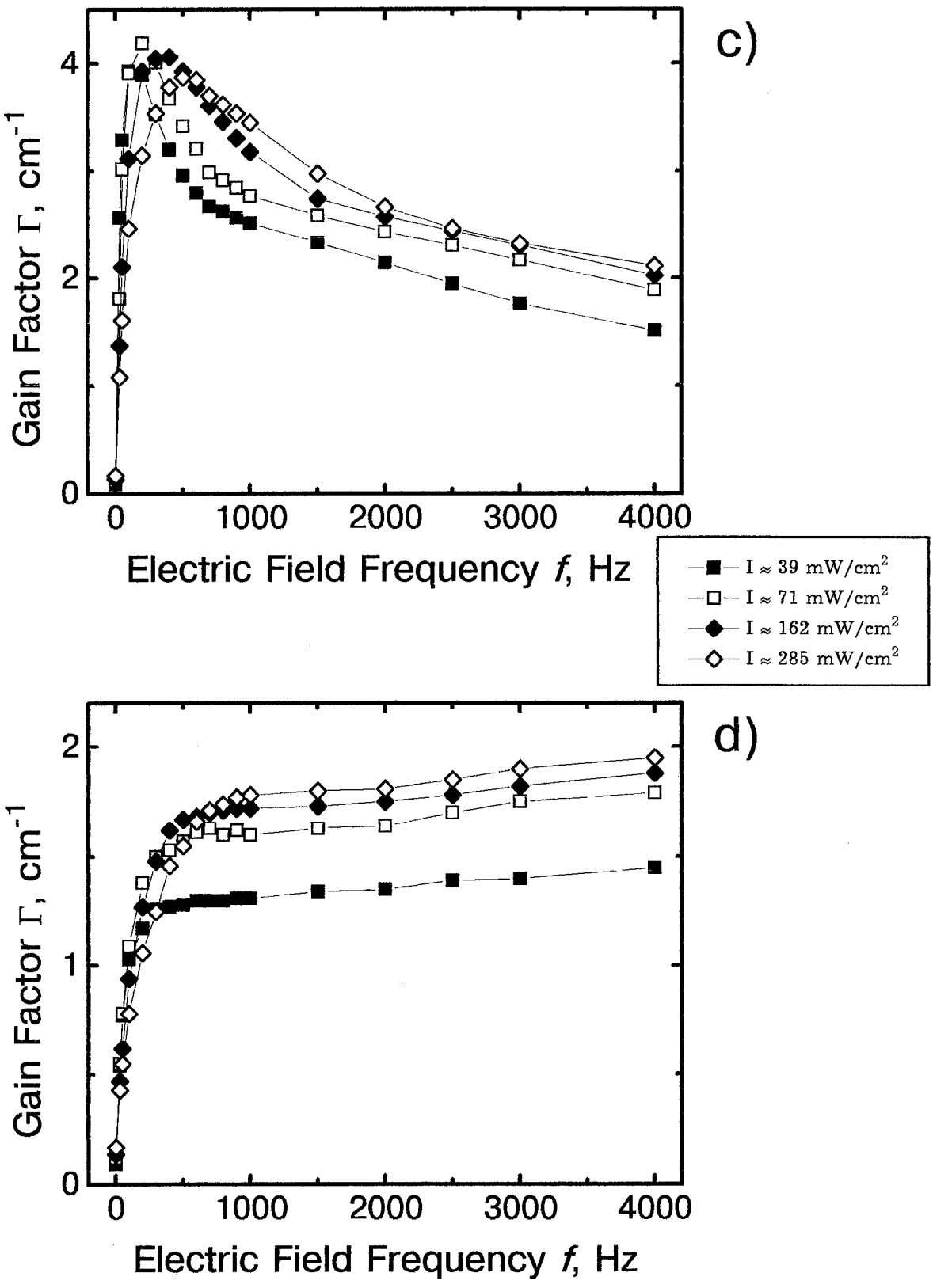

Fig. 3.3. Gain factor as a function of applied field frequency for Λ = 4.4 μm and for different intensities;
(c) - slew-rate waveform;
(d) - sine waveform.

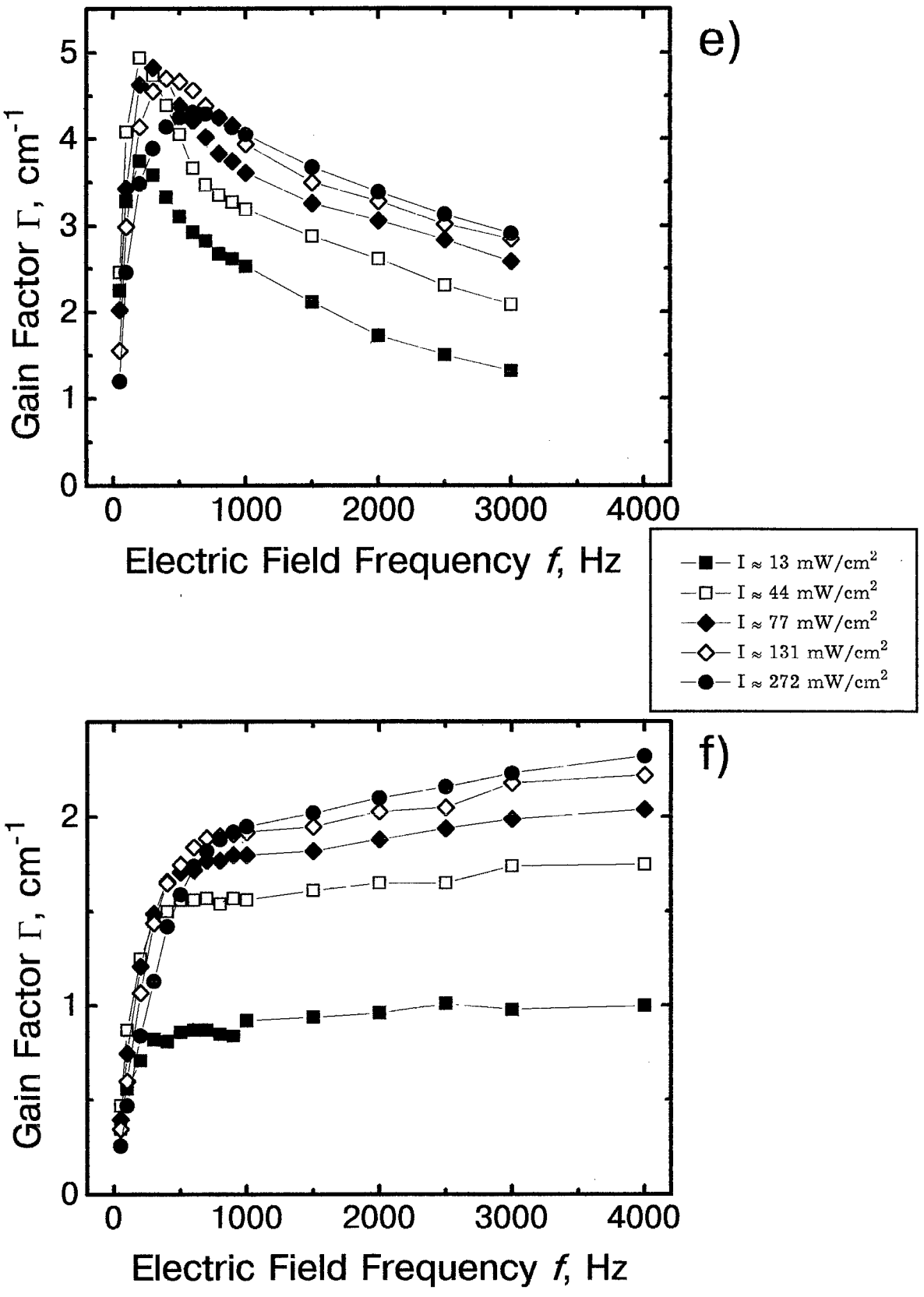

Fig. 3.3. Gain factor as a function of applied field frequency for $\Lambda = 8$ μm and for different intensities;
(e) - slew-rate waveform;
(f) - sine waveform.

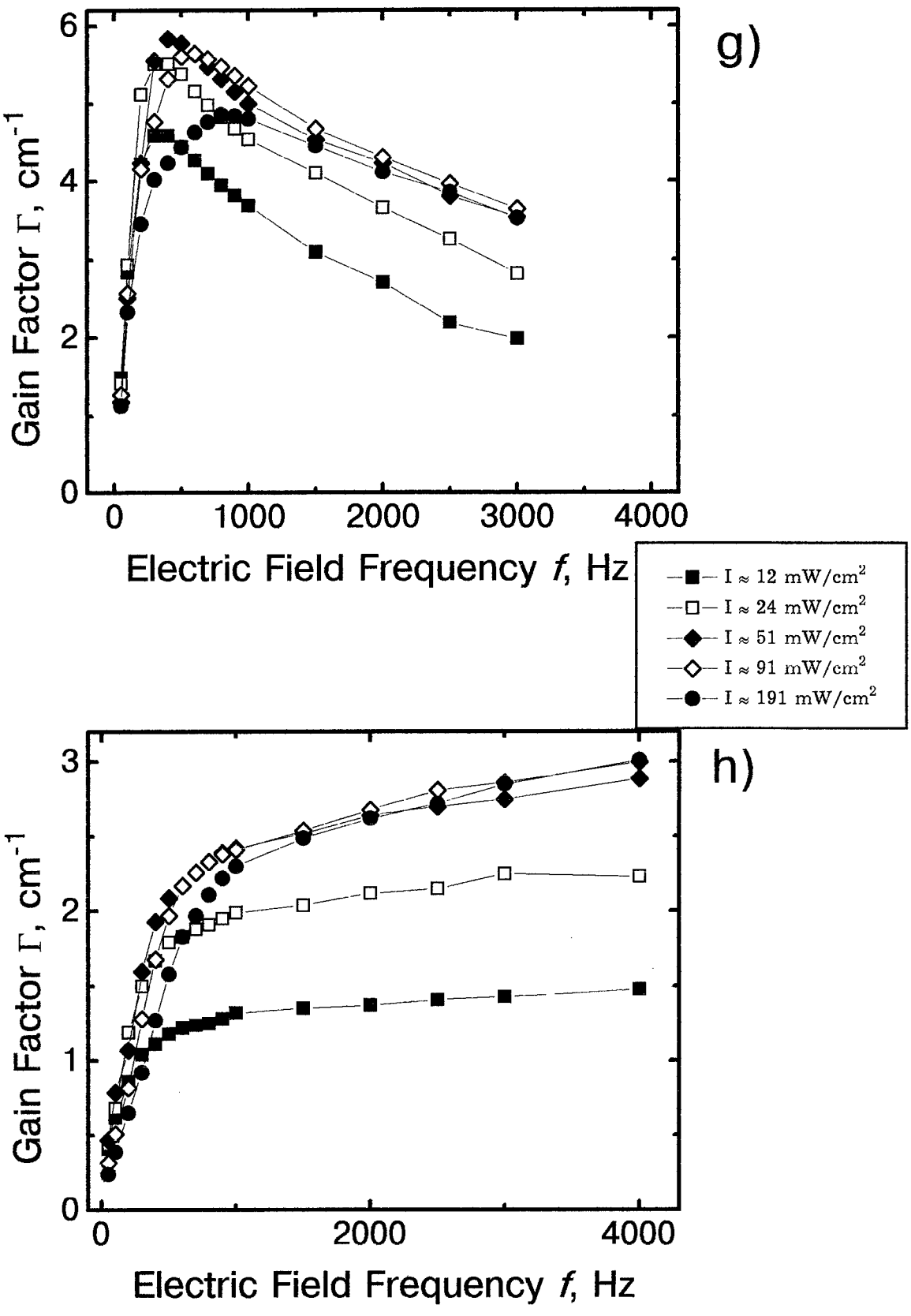

Fig. 3.3. Gain factor as a function of applied field frequency for Λ = 14 μm and for different intensities;
(g) - slew-rate waveform;
(h) - sine waveform.

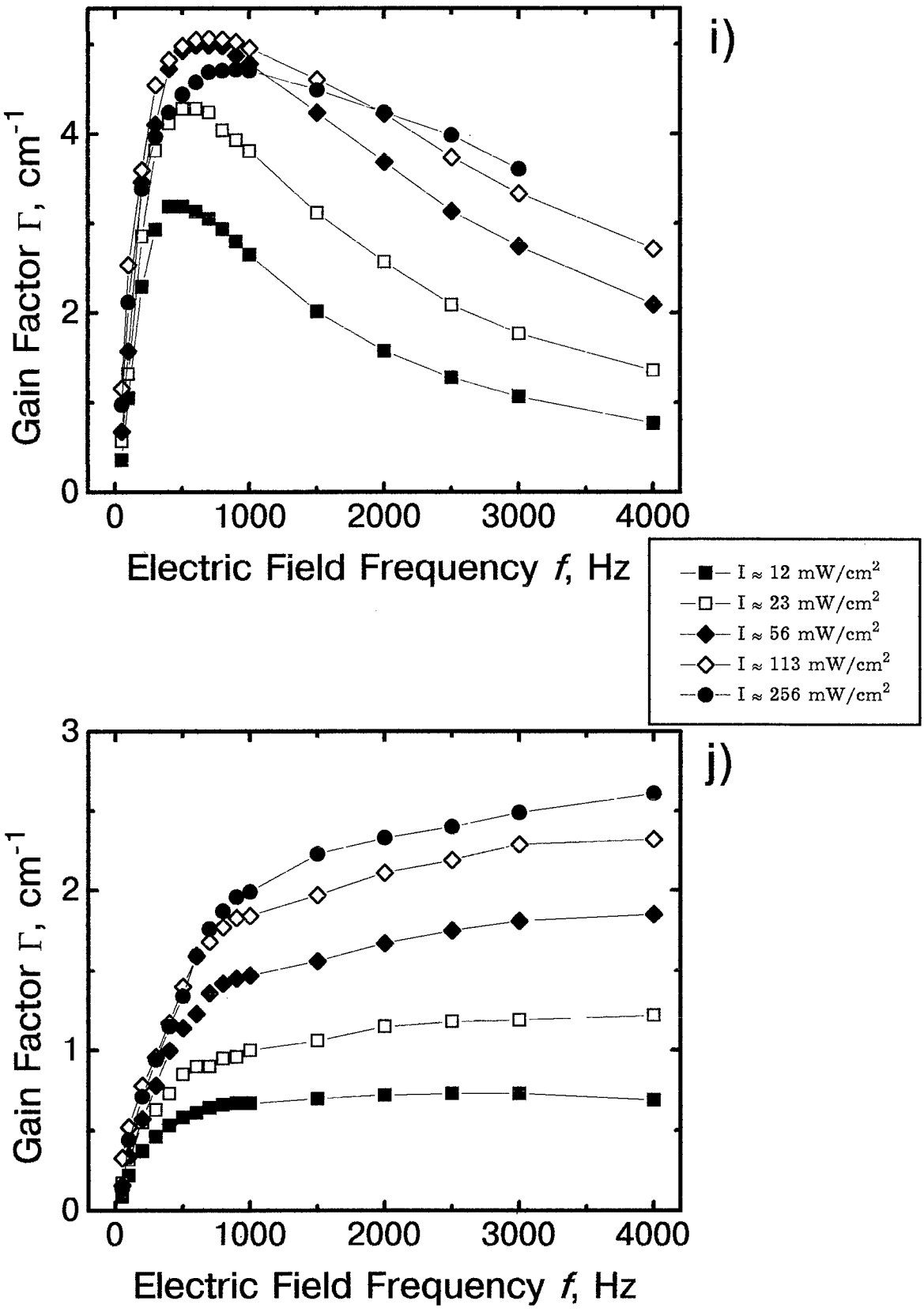

Fig. 3.3. Gain factor as a function of applied field frequency for Λ = 19 μm and for different intensities;
(i) - slew-rate waveform;
(j) - sine waveform.

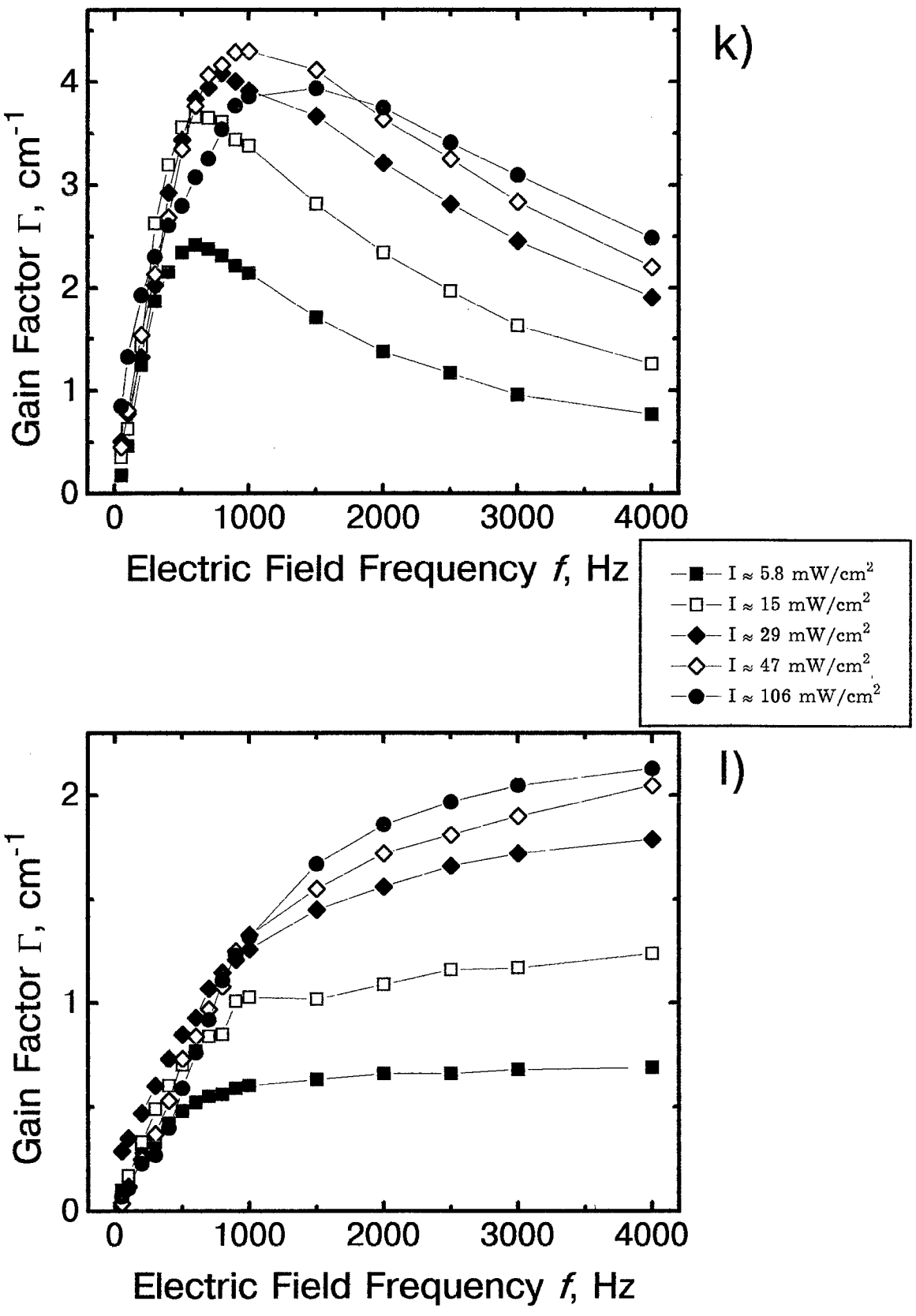

Fig. 3.3. Gain factor as a function of applied field frequency for $\Lambda = 30$ μm and for different intensities;
(k) - slew-rate waveform;
(l) - sine waveform.

$$I_0(P) = \frac{2}{T}\int_0^{\frac{T}{2}} \frac{P}{1+P^2q^2(t)}dt, \qquad (3.4)$$

and q(t) is a function describing the shape of field modulation with temporal period equal to T.

Thus to compare the amplitudes of the space-charge fields for external field with Slew-Rate-Limited Square Waveform characterized by parameter R and space-charge field with perfect square-shaped modulation (R = 0). For the case far from trap saturation it is convenient to introduce the parameter S = $\eta_{SR}/\eta_{Sq.}$ where η_{SR} and η_{Sq} are η-coefficients for Slew-Rate-Limited Square Waveform and for perfect square-shaped waveform, respectively.

Figure 3.4 represents the calculated values (dots) of S factor for different frequencies of the Slew-Rate-Limited Square Waveform (different R) for the grating spacings of particular measurements, external field amplitude 8.8 KV/cm and mobility-lifetime product evaluated before ($\mu\tau$ = 6×10^{-7} cm^2/V). The solid lines represents the similar calculations for the sinusoidal applied field for the same set of parameters.

The plotted S curves are calibration curves the deviation from the perfect square-shaped waveform taking into account. By dividing the measured value of Γ to calculated for the same conditions S one can estimate the ultimate gain factor which could be obtained for ideal square-shaped AC field. This correction has been done and the results for $\Lambda \approx 4.4$ μm and $\Lambda \approx 4.4$ μm are presented in Fig. 3.5a,b. It is clearly seen that for larger grating spacing the saturation of the gain factor becomes with the highest frequencies. Some deviations of the maximum values of the curves with rather high

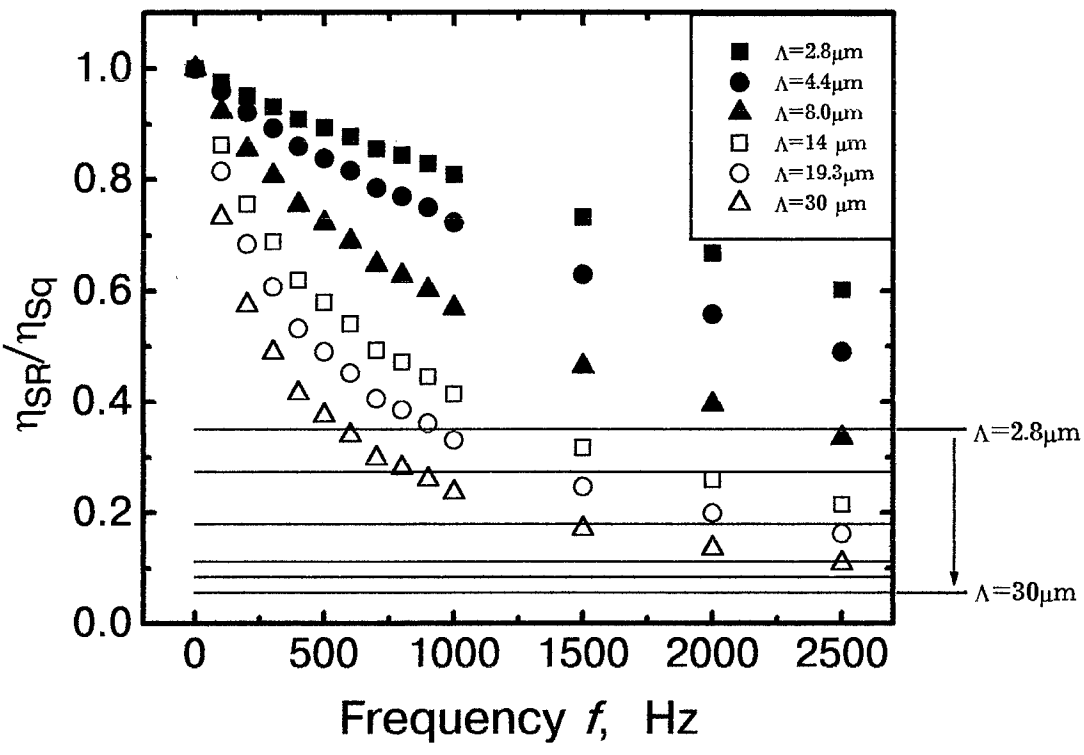

Fig. 3.4 Calculated S -factor
Slew-Rate waveform (marks)
Sine waveform (lines)

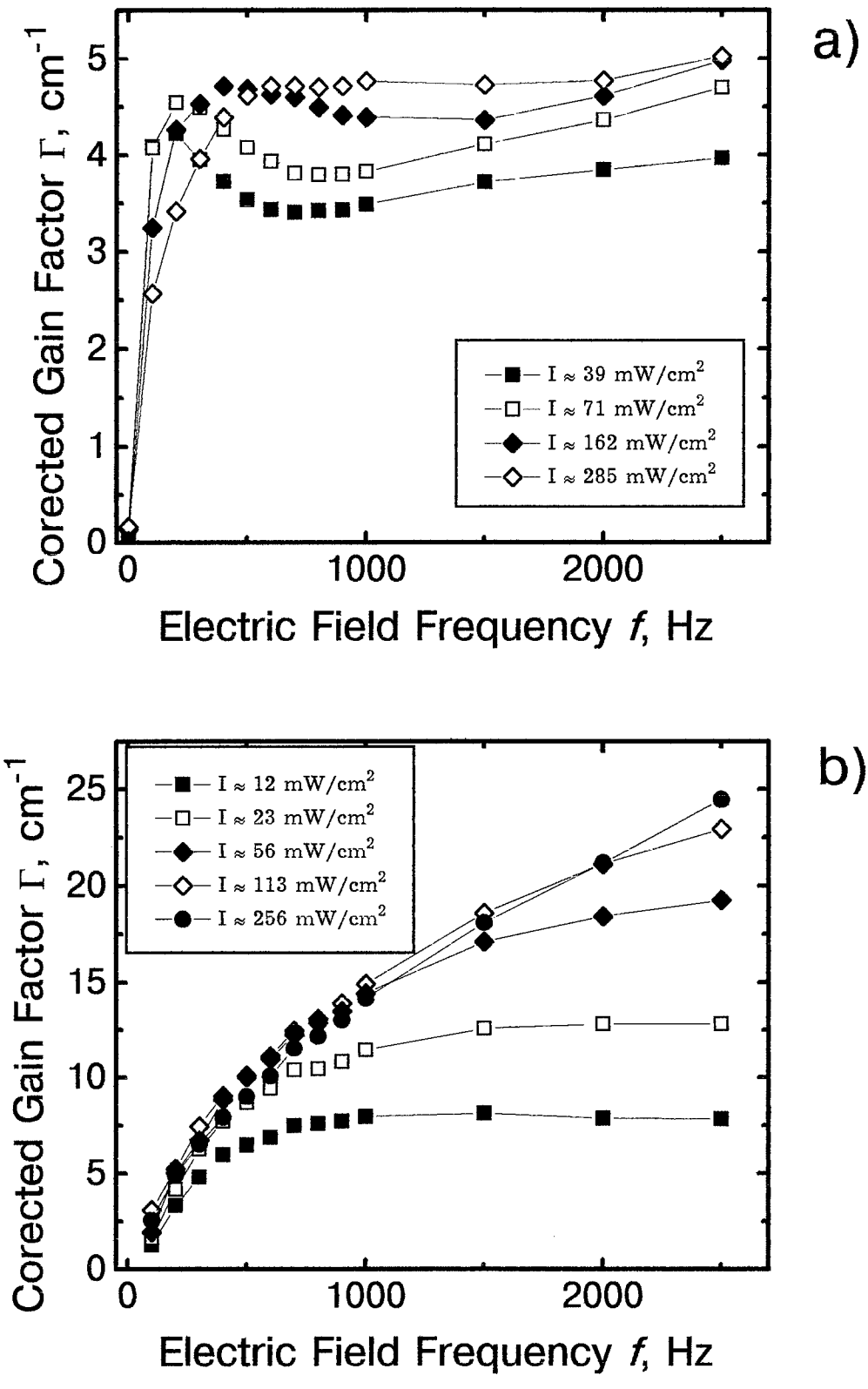

Fig. 3.5. Correction of the gain factor with slew-rate waveform to obtain ultimate hypothetical value for perfect square waveform;
(a) - Λ = 4.4 μm;
(b) - Λ = 19 μm;

intensity are caused by the error of calculation. Note that the maximum value of Γ about 20 cm^{-1} is reasonable value of gain factor in the case of beam-coupling in CdTe with perfect square field applied.

For large trap density that we have there is no saturation of gain factor neither with the increasing spatial frequency nor with the increasing applied field. So with the diminishing grating spacing and fixed amplitude of an applied field the gain factor should not decrease. Nevertheless we observe such a decrease both for the large and for small modulation frequencies (Fig.3.1). Fig. 3.6a represents by solid squares the dependence of gain factor Γ on grating spacing with the applied sinusoidal field. We took the maximum values of Γ for any given value of spacing from the dependences shown in Fig. 3.3 for largest modulation frequency of sinusoidal modulation, i.e., we supposed that the gain factor is already saturated both in intensity and in modulation frequency. The open squares shows the similar dependence for square-shaped modulation; for this curve we took the largest values of Γ from Fig 3.3, corresponding to different modulation frequencies. These experimental dependences and those measured earlier for the electric field with larger frequency do not fit to the theoretical dependences from Refs. 3.1 and 3.2.

The solid lines in Fig. 3.1 show the results of calculation from data of [3.1, 3.2] with previously measured $\mu\tau$ and l_S but with strongly reduced ξ = 0.43. These calculated curves are satisfactory describing the measured data for large grating spacings but they differ qualitatively for small spacings.

This disagreement as in the case with no applied field can be attributed to bipolar conductivity of the sample, i.e., by the dependence of ξ (see Eq. 1.4)

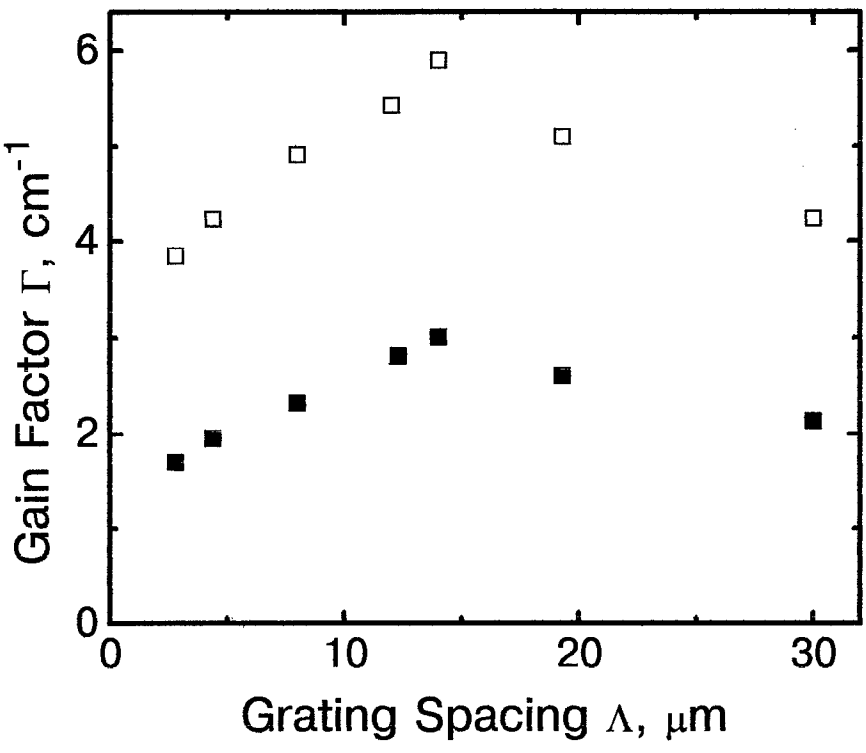

Fig. 3.6. Grating spacing dependence of gain factor with external electric fields

- ■ sine waveform;
- □ slew-rate waveform.

on grating spacing. For rather high applied field the value of ξ is a function not only of grating spacing but also of the applied field [3.6, 3.7]. In these conditions for higher applied field a detectable change of a factor ξ starts at higher grating spacings. For grating spacing Λ going to infinity the ultimate value of ξ depends on the applied field for the constant ratio of the diffusion lengths for carriers with different signs.

This is why we attribute just to bipolar conductivity both the fall-off of the gain factor at larger grating spacings with the applied field (comparing to the case with no field) and the shift of the gain maximum to larger grating spacings with the increasing amplitude of the applied field. We have yet not completed the calculation of spatial frequency dependence and field dependence for ξ because of uncertain choice of the model of volume space-charge formation.

With the increasing amplitude of the applied field the space-charge amplitude is linearly increasing until the trap-limited value is reached. Fig. 3.7 represents the electric field dependence of the gain factor Γ for the applied sinusoidal field, for two grating spacings, $\Lambda \approx 2.8$ μm and $\Lambda \approx 12.3$ μm. There is no saturation of gain factor with the increasing field in both curves. The solid lines shows the result of calculation within a model of [3.1,3.2] with several different ξ factors. The linear growth of the gain factor Γ for small grating spacings indicates just the variation of ξ with grating spacing and not a trap saturation as could be expected.

Similar dependences have been measured also for square-shaped field, with only exception that for all voltages used we took the largest value of gain

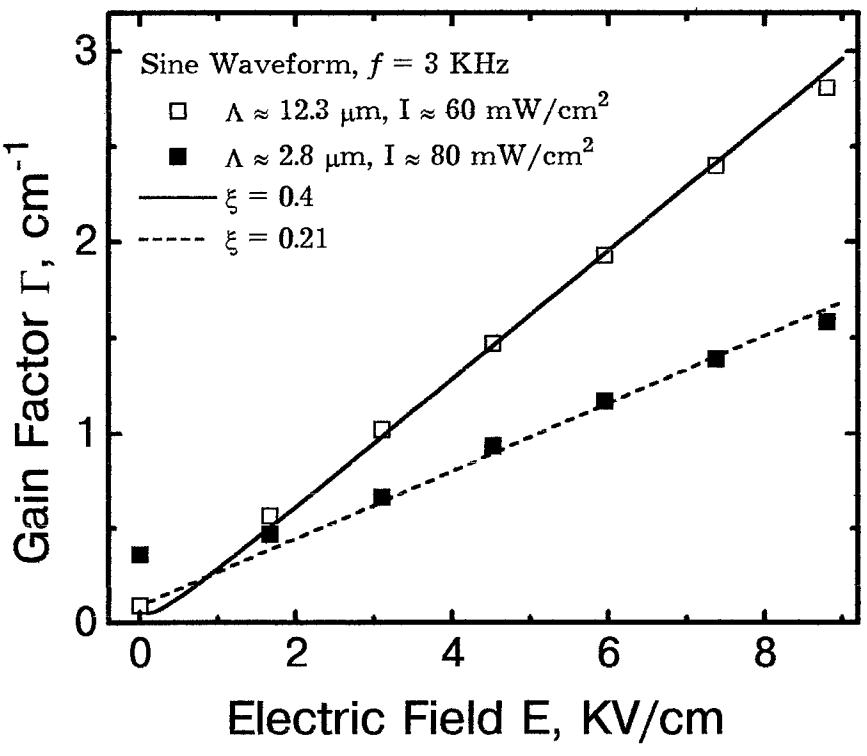

Fig. 3.7. Gain factor dependence on amplitude of sinusoidal applied electric field for $\Lambda = 2.8$ μm and $\Lambda = 12.3$ μm

factor. Fig. 3.8a,b shows the experimentally measured temporal frequency dependences of the gain factor Γ for several amplitudes of the square-shaped field measured at the same spacings $\Lambda \approx 2.8$ μm (a) and $\Lambda \approx 12.3$ μm (b).

Fig.3.9 shows the largest values of the gain factor Γ as a function of the applied field. In spite of the fact that these data correspond to different frequencies, the R-factor is changing only slightly for them because with the decreasing voltage the quality of square-shaped modulation becomes better (R defined in Fig. 3.2 was diminishing). These dependences as in the case of sinusoidal modulation are nearly linear; one of them is measured at relatively small grating spacing $\Lambda \approx 2.8$ μm which is nevertheless much larger then Debye screening length.

Let us compare now the values of the gain factor for small and for large modulation frequencies of the applied field. From Fig. 3.1 we can state that $\xi = 0.43$ both for E = 6 KV/cm and E = 3.1 KV/cm. From the dependence of the gain factor at $\Lambda \approx 12.3$ μm on applied sinusoidal voltage we evaluate $\xi = 0.4$ (from spacing where gain factor is not yet decreasing or ξ is no more Λ-dependent). Thus we conclude that the efficiency of photorefractive grating is nearly the same for the same amplitudes of high-frequency or low-frequency sinusoidal field. This permits us to suppose that the gain factor is nearly constant in frequency range from $f_{min} \approx 3$ KHz to $f_{max} \approx 18$ Khz for intensity used.

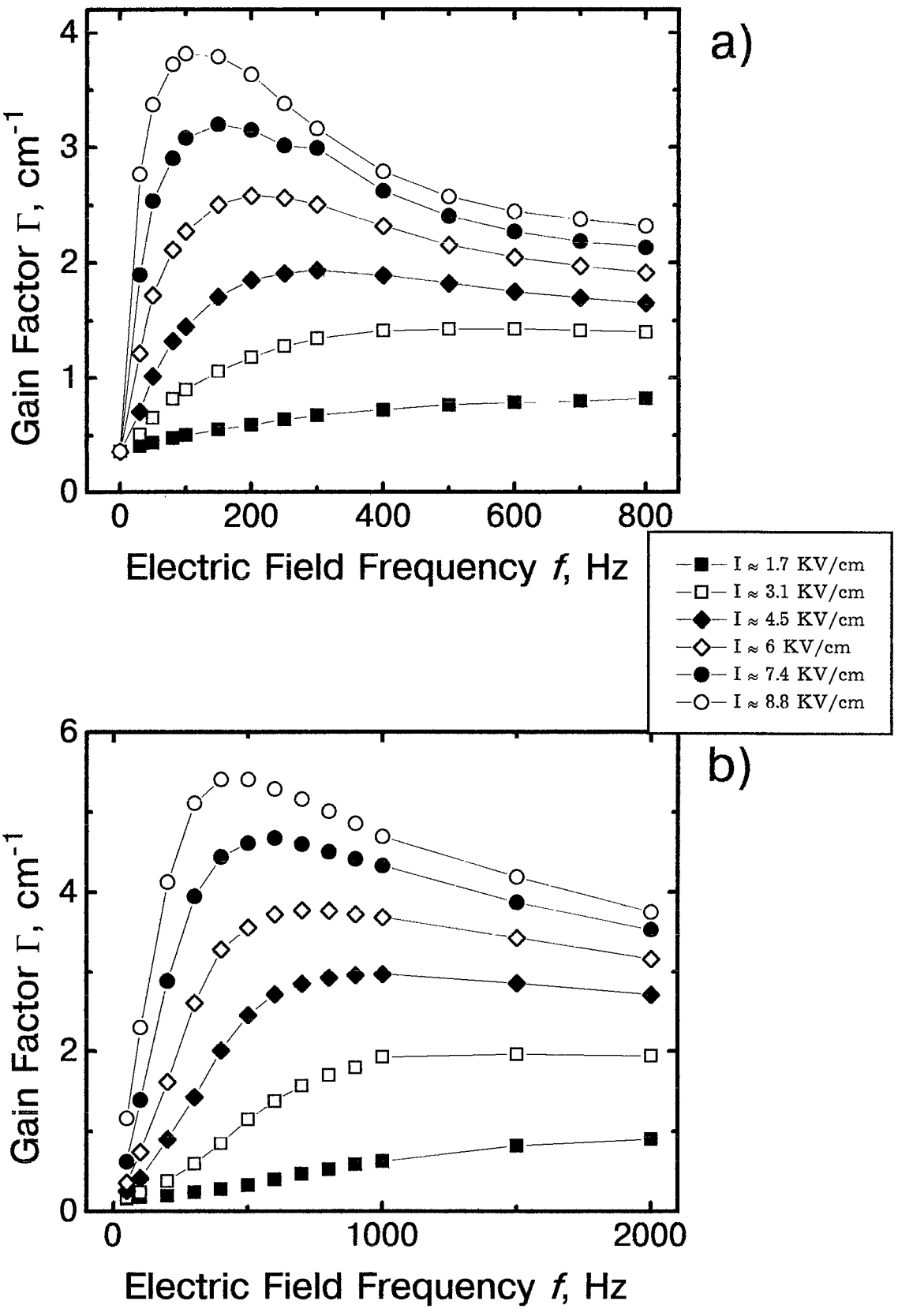

Fig. 3.8. Frequency dependences of gain factor for different voltage;
(a) - $\Lambda \approx 2.8$ μm, $I \approx 80$ mW/cm^2;
(b) - $\Lambda \approx 12$ μm, $I \approx 60$ mW/cm^2.

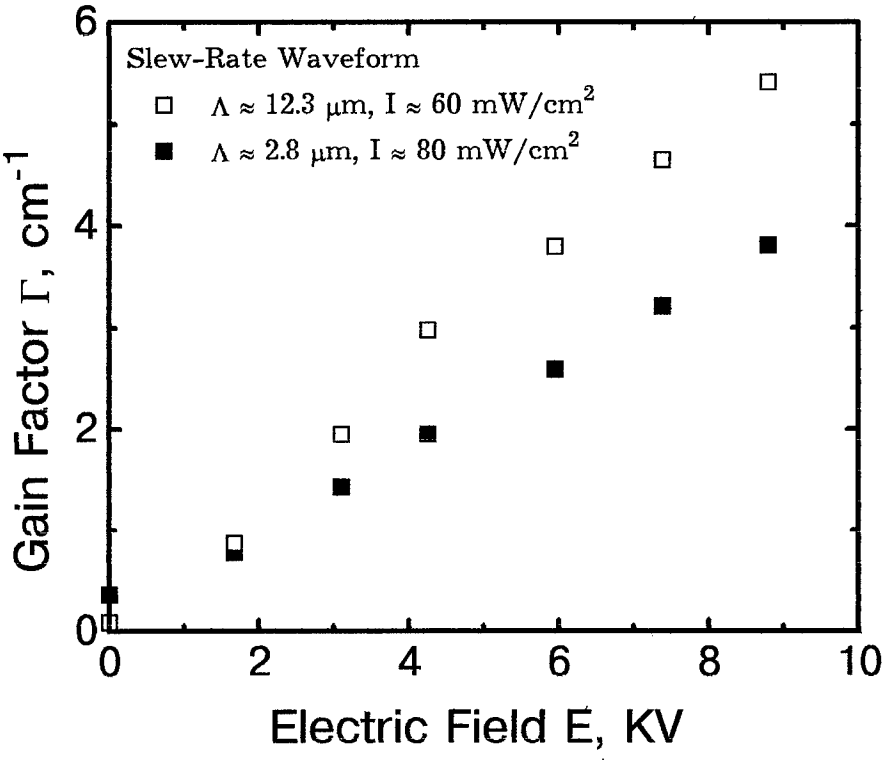

Fig. 3.9. Gain factor dependence on amplitude of slew-rate waveform applied electric fields for $\Lambda = 2.8$ μm and $\Lambda = 12.3$ μm

3.3. "Net" gain due to beam-coupling in CdTe.

We examine further the values of the gain factor that we got. The largest coupling strength measured in our experiments is $\Gamma d \approx 3.8$ for interaction length in the crystal $d \approx 0.65$ cm. For so strong interaction the gain factor should be a function of the beam intensity ratio, first of all because of depletion of the strong pump wave. To evaluate the largest gain factor which is no more intensity ratio dependent we measure the dependence of the gain factor on beam intensity ratio, $\beta = I_p/I_s$ for nearly optimum grating spacing $\Lambda \approx 12.3$ μm (see Fig. 3.10). For this spatial frequency the largest beam intensity ratio was $\beta \approx 1000$. As it has been already mentioned we were unable to use larger β because of rather strong scattering.

The largest gain factor measured for the smallest contrast of fringes of interacting waves was $\Gamma \approx 6.3$ cm^{-1} (compare with the absorptivity $\alpha \approx 1.2$ cm^{-1} at 1.06 μm. This value of gain factor is exceeding nearly to 40 % that measured previously at the same voltage (8.8 KV/cm) in vanadium doped cadmium telluride [3.9].

Figure 3.11 represents the dynamics of the light intensity for weak beam transmitted through the sample with the square-shaped 8.8 KV/cm electric field applied at $\Lambda \approx 12.3$ μm and with $\beta \approx 300$. The intensity here is normalized to the intensity of the signal wave incident to the crystal. It can be seen that in spite of Fresnel losses and absorption losses the signal wave gets 8 times amplified because of direct coupling to the strong pump wave.

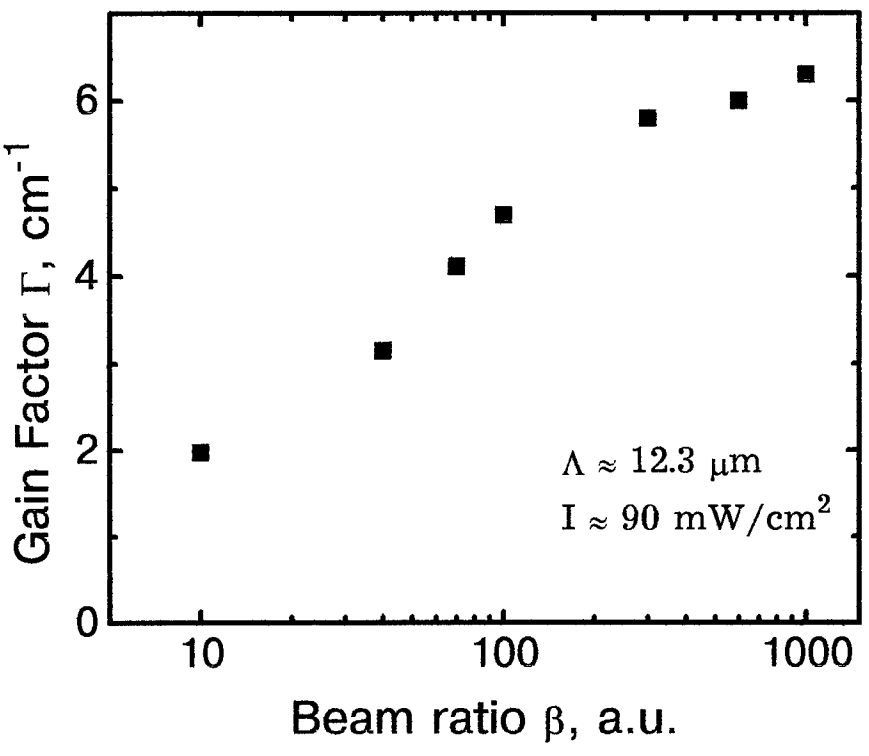

Fig. 3.10. Gain factor as a function of signal to pump beams intensity ratio.

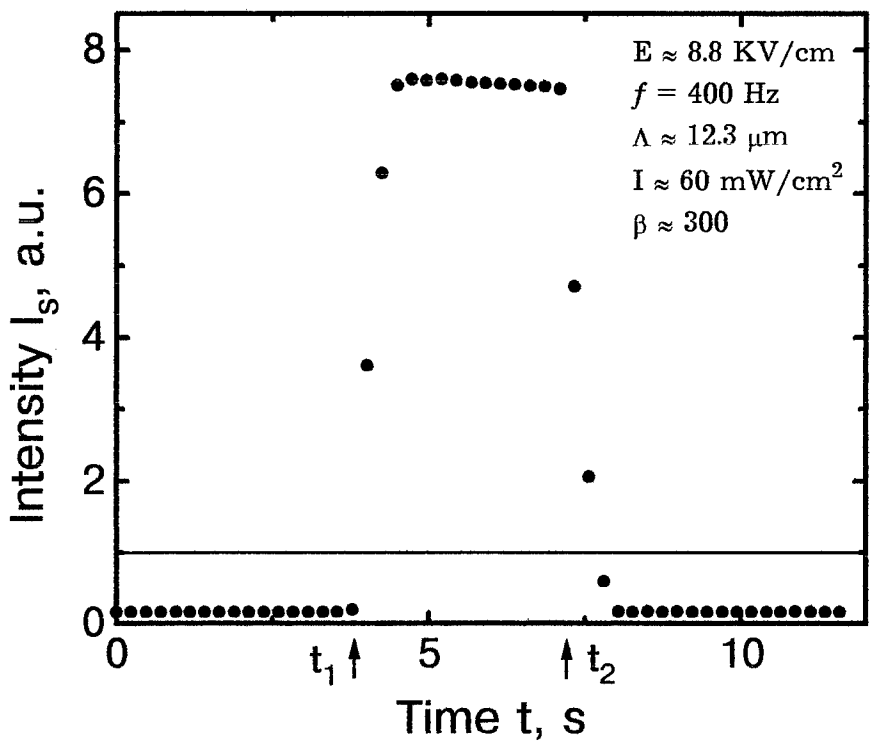

Fig. 3.11. Dynamics of signal beam when electric fielf is applied;
t_1 - Electric Field On
t_2 - Electric Field Off.

REFERENCES TO SEC 3

3.1. S. I. Stepanov and M. P. Petrov, Opt. Comm. **53**, 292 (1985).

3.2. K. Walsh, A. K. Powell, C. Stace, and T. J. Hall, JOSA B **7**, 288 (1990).

3.3. J. Kumar, G. Albanese, W. H. Steier, and M. Ziari, Opt. Lett. **12**, 120, (1987).

3.4. K. Walsh and T. J. Hall, Appl. Opt. 28, **16** (1989).

3.5. M. Ziari, W. H. Steier, P. M. Ranon, M. B. Klein, and S. Trivedi, JOSA B **9**, 1461 (1992).

CONCLUSIONS

Cadmium telluride doped with germanium is a promissing photorefractive crystal for use with Nd :YAG lasers. With relatively small absorptivity at 1.06 μm ($\alpha \approx 1.2$ cm^{-1}) it can assure:

(I) the gain factor $\Gamma > 2$ cm^{-1} and net amplification of the weak signal beam in geometry of coupling of two counterpropagating waves with no applied field;

(2) the gain factor $\Gamma \approx 6.3$ cm^{-1} and nearly one order of magnitude high net gain of the weak signal beam in geometry of coupling of two copropagating waves with square-shaped AC field (8.8 KV/cm).

According to our estimates the studied crystal may assure even much more impressive gain factor up to 20 cm^{-1} in case of perfect square-shaped AC field. To get so high gain one should solve the severe technical problem of generation of high-voltage high-frequency ideal rectangular pulses.

The other possible way to get higher gain factors is the modification of crystal growth procedure aiming production of high-resistant crystals with monopolar conductivity.

The success of our efforts in getting high gain with the applied AC field is assured in part by Synthesized Function Generator Stanford Research Systems Model DS345 and High Voltage Trak Amplifier Model 609C-6 purchased within the present EOARD project.

The results of this study are described in the article

S. G. Odoulov, A. N. Shumelyuk, G. A. Brost, and K. M. Magde, "Enchancement of beam coupling in near infrared for Tin Hypotiodiphosphate"

sent for publication to **OPTICS LETTERS**

and are presented in to two Conferences:

- SPIE VI International conference - NOLPC'95

"Nonlinear Optics of Liquid and Photorefractive Crystals",

October 1995, Ai-Danil, Crimea.

- SPIE International conference

"Holography, correlation optics and storage materials",

May 1995, Chernivtsy, Ukraine.

Two other articles:

G. A. Brost, K. M. Magde, S. G. Odoulov, and A. N. Shumelyuk, "Spectral sensitivity of photorefractive $Sn_2P_2S_6$" and

S. G. Odoulov, K. V. Shcherbin, A. N. Shumelyuk, G. A. Brost, and P. M. Fochouk, "Beam-coupling in germanium doped CdTe crystals"

are now in preparation for sending to publication.